

Guava Fruit Ripening Optic Inspection System by Means of Digital Image Analysis

Andrés G. Marrugo Hernández

This work was submitted by Andrés G. Marrugo Hernández
in partial fulfillment of the Requirements for the Degree of
Ingeniero Mecatrónico

Supervisor: Lenny A. Romero Pérez, MSc.

Mechanics and Mechatronics Engineering Department
Universidad Tecnológica de Bolívar
October, 2007

Guava Fruit Ripening Optic Inspection
System by Means of Digital Image Analysis

by

Andrés Marrugo
Universidad Tecnológica de Bolívar

October, 2007

This document was prepared using MiKTeX 2.5, 2006.

*to Chachi, Javier, María Emma,
Juan Javier and Alexandra.*

Acknowledgements

I am grateful to my research advisor Professor Lenny Romero for facilitating the completion of my degree in Mechatronics Engineering while working full time with the basic science department. I am always inspired by her penchant for research and this work is evidence of that attitude, because work performed under this project is out of scope of her contractual obligations.

I would like to thank Dr. Franco for offering his comments on this work, especially on the statistical analysis. I would also like to thank the research group *Proyectos Alimentarios* of the Universidad de Cartagena for their collaboration in the physical-chemical measurements and the head of the Social Communication department of the Universidad Tecnológica Prof. Jose Ricardo Escobar for his support on lending us the photography lab to do the experiments. I truly thank the initial support of the professors Sonia Contreras and Juan C. Martínez.

I sincerely appreciate the support of my family, Chachi, Javier, María Emma and especially Juan Javier for his comments, suggestions and for his aide in the image acquisition procedure. I also wish to thank Dr. Vivas for his support, Dr. Villa and Dr. Sarria for their comments. I wish to thank as well Dr. Useche for his willingness to review and evaluate this work.

A final acknowledgement goes to Professor Richard Feynman whom I never met in person but whose legacy expands beyond his death. It is this legacy what has endowed me with a new vision of nature: *The scientist's perception*.

Contents

List of figures	iv
List of tables	v
Summary	vi
Introduction	1
Research Aims	2
1 Literature review	3
1.1 Ripeness (Maturity)	3
1.2 Destructive testing (DT) methods	4
1.2.1 Mechanical Methods	5
1.2.2 Physical-chemical methods	6
1.2.3 Sensory or Subjective Measurements	9
1.3 Non-destructive testing (NDT) methods	10
1.3.1 Electromagnetic technologies	10
1.3.2 Mechanical technologies	17
1.3.3 Electrochemical technologies	19
1.4 Machine vision and fruit sorting	19
1.4.1 Components of a machine vision system	20
1.4.2 Image acquisition	21
1.4.3 Fruit sorting	22
1.5 Digital image processing	26
1.5.1 Digital image and basic concepts	26
1.5.2 Spatial and gray-level resolution	27
1.5.3 Basic Relationships Between Pixels	28
1.5.4 Color and color models	31
1.5.5 Digital image processing techniques	34
1.5.6 Color content-based image classification	40

2	Experimental design	42
2.1	Overview	42
2.2	Proposed system	43
2.2.1	Materials	43
2.2.2	Assembled system	44
2.3	Image processing algorithm	47
2.3.1	Image segmentation	47
2.3.2	Spline-Interpolation based contour detection	49
2.3.3	Color feature extraction	51
2.4	Guava fruit testing	51
2.5	The similarity approach	52
3	Results	54
3.1	Destructive testing	54
3.1.1	Evolution of total soluble solids	54
3.1.2	Titrateable acidity	55
3.1.3	Maturity Index	55
3.2	Non-Destructive testing	56
3.3	Data analysis	59
3.3.1	A first descriptive analysis	59
3.3.2	Statistical analysis	60
3.4	Discussion	71
4	Conclusions	72
4.1	Future work	72
A	Statistical analysis	73
A.1	Regression model selection	73
A.1.1	MSE	73
A.1.2	R-Squared	74
A.1.3	Adjusted R-Squared	74
A.1.4	Cp	74
A.2	Multifactor ANOVA	75
B	Mathematical Tools	77
B.1	The L1-distance	77
B.2	The similarity matrix	77

List of Figures

1.1	Typical climacteric fruit respiration behavior.	4
1.2	Photo of a Handheld Refractometer.	7
1.3	Titration apparatus.	8
1.4	Incident light on a fruit.	11
1.5	CIE L*a*b* color space.	12
1.6	Visible and near infrared interactance spectrum.	13
1.7	Potato MRI.	16
1.8	Visualisation of the experimental setup. (Mizrach et al. [1]).	18
1.9	Visualisation of input ultrasonic waveform and the fourier transform of that waveform. (Mizrach et al. [1]).	18
1.10	Components of machine vision system. (McConnell et al. [2]).	21
1.11	The three principal sensor arrangements used to transform illumination energy into digital images. (Gonzalez and Woods [3]).	23
1.12	An example of the digital image acquisition process.	24
1.13	Intelligent fruit sorting system. (Feng et al. [4]).	25
1.14	Illumination chamber. (Pla et al. [5]).	25
1.15	Coordinate convention used to represent digital images. (Gonzalez and Woods [3]).	27
1.16	A 1024×1024 , 8-bit image subsampled down to size 32×32 pixels. The number of allowable gray levels was kept at 256. (Gonzalez and Woods [3]).	28
1.17	(a) 452×374 , 256-level image. (b)-(d) Image displayed in 32, 16, and 2 gray levels, while keeping the spatial resolution constant. (Gonzalez and Woods [3]).	29
1.18	Pixel neighbourhoods. (Cattin [6]).	30
1.19	The pixels p, q are not connected under 4-connectivity but they are under 8-connectivity. (Cattin [6]).	31

1.20	Schematic of the RGB color cube.	32
1.21	The CIE LCH color space.	33
1.22	Image segmentation via thresholding.	38
1.23	A 3×3 structuring element	39
1.24	Effect of erosion using a 3×3 square structuring element. (Fisher et al. [7])	40
2.1	Parallax continuous rotation servo.	44
2.2	Assembled optic inspection system.	45
2.3	Block diagram of the assembled system.	46
2.4	Capture GUI program.	47
2.5	Result of image segmentation.	48
2.6	Result of blob algorithm.	49
2.7	Process and result of interpolation based contour detection.	50
2.8	Similarity procedure.	53
3.1	Total soluble solids content of <i>P. guajava</i> during storage at ambient conditions.	55
3.2	Titrateable acidity of <i>P. guajava</i> during storage at ambient con- ditions expressed as % of citric acid.	56
3.3	Maturity index (I_m) of <i>P. guajava</i> during storage at ambient conditions.	57
3.4	Segmented images of different guavas used for the PCC mea- surements.	58
3.5	Predominant color content evolution in 10 guavas from the control group.	59
3.6	Normalized predominant color content evolution in 10 guavas from the control group.	60
3.7	Maturity index and average PCC evolution.	61
3.8	Adjusted R^2 plots for TSS, TA and I_m	63
3.9	TSS and TA scatterplot by level Code.	64
3.10	Box and whisker plots.	69
3.11	Quantile-Quantile plots.	70

List of Tables

1.1	Stacking Procedure	37
3.1	Generalized forms of the best TSS, TA and I_m fit models in terms of color values (L, a, b, c, h)	61
3.2	Statistical results of the best models for determining TSS, TA and I_m	62
3.3	TSS and TA levels.	65
3.4	Analysis of Variance for h - Type III Sums of Squares. “h” stands for PCC measured in hue degrees.	65
3.5	Tests for Normality using the Kurtosis Z-score test.	66
3.6	Summary statistics.	67
3.7	Comparison of means TSS1 - TSS2.	67
3.8	Comparison of means TA1 TA2.	67
3.9	Comparison of means I_{m1} - I_{m2}	68
A.1	An example of an analysis of variance for “minutes” - Type III Sums of Squares.	75

Guava Fruit Ripening Optic Inspection System by Means of Digital Image Analysis

Andrés Guillermo Marrugo Hernández
agmarrugo@gmail.com
Universidad Tecnológica de Bolívar, 2007

Supervisor: Lenny A. Romero Pérez, MSc.
lromero@unitecnologica.edu.co

Summary

The agriculture industry is profoundly affected by subjectivity in quality inspection of fruits and vegetables. Quality in fruits is typically determined on a sample of the total population by destructive means and inference is performed on the rest of the population. Due to these factors non-destructive testing of fruits and vegetables has come forth and becoming an industry standard. Given that Guava (*Psidium guajava*) is a tropical fruit of major commercial impact in the country and in the region [8, 9], that is practically cultivated in every tropical and subtropical region of the world [10] the present work estimates its suitability for non-destructive testing. Non-destructive information from the fruit was acquired by means of digital image analysis and corroborated with traditional physical-chemical methods involving the measurement of total soluble solids (TSS) and titratable acidity (TA). Predominant color content (PCC) was determined, as well as its evolution, for identifying its relationship with TSS and TA. While TSS and TA behavior was as reported in literature and PCC behavior was as expected, no reliable relation was found probably due to the fruits respiration patterns. A similarity scheme was undertaken using color coherence vectors (CCV), an image color content retrieval algorithm, which assumes that two similar guava fruit images represent similar internal properties. This method shows recognizable correlation within the studied samples.

Introduction

In recent years the agriculture industry has become more aware of the advantages that technology brings in productive processes, from post-harvest to final consumer products. For this reason much effort is being put in research intended for improving production. Production excess and heavy market competition has endowed a new paradigm where quality succeeds quantity.

Quantitative evaluation of agricultural products has been of interest to researchers for many years. However, there is no clear definition of fruit quality. Quality is a human construct comprising many properties or characteristics. Quality of produce encompasses sensory properties (appearance, texture, taste and aroma), nutritive values, chemical constituents, mechanical properties, functional properties and defects. Some of these properties are excellent indicators of the ripeness degree and possible shelf-life[11].

To inspect maturity in fruits, traditionally a sample is taken from the total population. A series of tests are performed, such as chemical, organoleptic, mechanical, among other tests of destructive nature. Afterward an inference approach is performed on the rest of the population. The fact of not being able to determine fruit properties without its destruction and the need for a rapid and adequate classification of agricultural products has led to the development of non-destructive techniques, which allow the determination of the internal properties of the product without its destruction.

Non-destructive testing in fruits and vegetables has been around for about 30 years. The first tests were performed on apples by Abbot [12] and practical results were observed by calculating a stiffness coefficient, based on an acoustic test, using the first resonance frequency and the fruit's mass. Mizrach et al. [13]. built and evaluated a system for determination of the basic acoustic properties of some fruits and vegetables, i.e., wave propagation velocity and attenuation, and suggested using this technique for the non-destructive quality evaluation of fruits and vegetables. A fruit grading machine vision

system for color and size classification was developed by Pla et al. [5] with the disadvantage that the classification rules are predefined based on color ratios without any direct relation with a ripeness degree.

Currently, most machine vision sorting systems are designed to operate under predefined rules, sometimes based on subjective judge criteria, without proper knowledge of the physiology of the fruit and the relations between these properties.

Given that Guava (*Psidium guajava*) is a tropical fruit of major commercial impact in the country and in the region [8, 9], that is practically cultivated in every tropical and subtropical region of the world [10] we decided to study its suitability for non-destructive testing. The focus of this work is to investigate the possibility of determining an adequate machine vision model based on physiological parameters and a low cost architecture for the appropriate sorting of guava fruit. The technique involves digital image analysis corroborated with traditional physical-chemical methods involving the measurement of soluble solids and titratable acidity.

The following chapter covers the relevant literature that was accessible, including a brief introduction to the destructive methods in subsection.

Research Aims

The aim of the research described in this work is to investigate the pre-existing methods of image-based non-destructive fruit testing and to propose a solution to the problem of guava fruit testing using these methods and to provide evidence to support that such a system could be implemented in a real time environment to rapidly grade guava fruit maturity and assist in the quality sorting.

Chapter 1

Literature review

1.1 Ripeness (Maturity)

In post-harvest physiology mature or ripe is considered as the stage at which a commodity has reached a sufficient stage of development that after harvesting and post-harvest handling, its quality will be at least the minimum acceptable to the ultimate consumer (Reid cited in [14]). Fruit quality is a combination of attributes and properties that give them value in terms of human consumption.

Maturity indicators in guava fruit are softening of the flesh, decreasing acidity and increasing contents of sugar, soluble solids and total solids [15]. Chemical tests are an important means for determining the maturity of fruits, but firmness is the factor most closely related to the stage of maturity.

Ripening involves changes that transform the mature fruit into one ready to eat. Changes associated with ripening include loss of green color development of yellow, red and other characteristics of the variety. As fruits ripens, it softens, its acidity declines and it produces certain volatile compounds that give its characteristic aroma (Chapman [16]). Increased respiration and ethylene production rates are among the physiological changes associated with ripening [15]. Generally fruits are classified into climacteric and non climacteric. Guava fruit is classified as a climacteric one because it has patterns of respiration similar to the one shown in Figure 1.1. Climacteric fruits exhibit a respiratory behavior characterized by a decrease in the respiration rate until it reaches a minimum and then increases to a maximum or a peak, called the climacteric, to decrease once again and disappear with the death of the

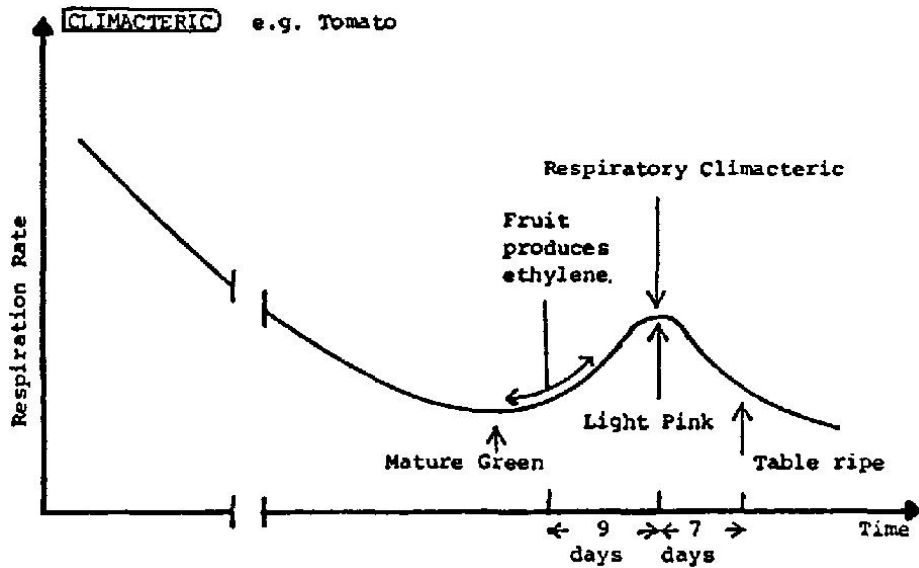


Figure 1.1: Typical climacteric fruit respiration behavior. From a FAO production manual [17]

fruit. Once the fruit ripens, senescence begins; physical and chemical changes continue after optimum ripeness is reached including further softening, loss of desirable flavor and complete breakdown.

When a relationship between chemical or physical changes and the fruit maturity have been established, potential maturity indices can be studied for their reliability whether for harvest or post-harvest quality determination. For the majority of fruits several possibilities have been suggested including, size, shape, color, firmness, soluble solids content and concentration of acids. Since most of the mentioned properties involve destructive testing methods these will be covered in the following Subsection.

1.2 Destructive testing (DT) methods

The majority of destructive testing methods are associated with the measurement of firmness based on the response to some external force. Chemical and biophysical tests can be categorized as DT methods as most of them seek to measure some internal property associated with fruit quality that requires partial or total destruction. Some of these methods are:

1.2.1 Mechanical Methods

Mechanical properties relate to texture. Texture can be described by sensory terms such as juicy, chewy, creamy, mealy, crispy, crunchy, etc. In the case of very soft produces the firmness can be described by viscosity, or consistency testing, that is, to measure some kind of resistance to a rotating probe, or rather to measure the torque [18]. Mechanical tests of texture include the familiar puncture, compression and shear tests, as well as creep and impact methods reviewed by Abbot [12]. Some of these tests are described below:

Puncture testing

The use of a small probe pressed into fruit flesh some distance. The maximum force recorded during this puncture is what is used to grade firmness. This tests leaves only a small mark o bruise (the size of the probe) on the object. Many different probes have been used over time, but one of the most common, is called the Magness–Taylor probe.

Shear testing

How much force is required for parallel planes of cells from a piece of fruit to slide across one another. The theory behind this is that the measured force gives an indication of the strength of the structure of the fruit.

Compression

The response to cells of the fruit being compressed, the point of failure or some point of deformation. Usually, failure occurs when the internal structure is forced apart, individual cells become crushed or often both.

Tension

Parts of, or a whole piece of fruit are stretched until failure. This failure can be caused by cell rupture, cell separation or both.

Torsion

The response of the fruit to twisting the fruit in some way. This form of testing is rarely used due to the difficulty of implementing a proper torsion test. However, a compromise is called the *twist test* which grabs the fruits

using a large spindle and rectangular blade and twists the fruit until failure. Considered to be, in effect, a combination of Compression and Tension testing.

The most common of the above methods is the Puncture test. This is due to the ease of applying such a test, the low damage caused and the reasonably high accuracy as described by Abbott [12].

1.2.2 Physical-chemical methods

Establishing fruit maturity demands a physical-chemical analysis in which several properties must be determined, such as, total soluble solids (TSS), titratable acidity (TA), ionic acidity (pH), among others. In addition, relative maturity indices can be determined by the relationships that exist between these properties.

Teotia (cited in [10]) found a close relationship between the TSS, TA, sugar content, starch and specific gravity with fruit maturity and quality. The individual determination of the most important guava fruits sugars, such as: glucose, fructose, sucrose, etc., as well as the pH, TA and texture has become an essential study. Further research is being conducted in the fields of genetics and biochemical mechanisms in the formation of this product [10, 20, 21].

Simple sugars content

As ripening approaches, complex sugars transform into simple sugars and acids become esters or sugars. A refractometer is employed to measure them by means of light refraction. The apparatus consists of two prisms where a drop of juice is placed in order to determine its sugar content. Internally the refractometer has a scale in degrees Brix ($^{\circ}\text{Brix}$ = percentage of sucrose) and according to the refraction of the light that goes through the prisms and the juice sample a measurement of the TSS can be made directly from the scale (see Figure 1.2). The more the fruit ripens the greater the TSS value will be [22].

Cañizares et al. [23] found that as the fruit approaches maturity the TSS content increases and it is attributed to the conversion of starch to sugars, probably due to the increase of the starch hydrolase enzymes.

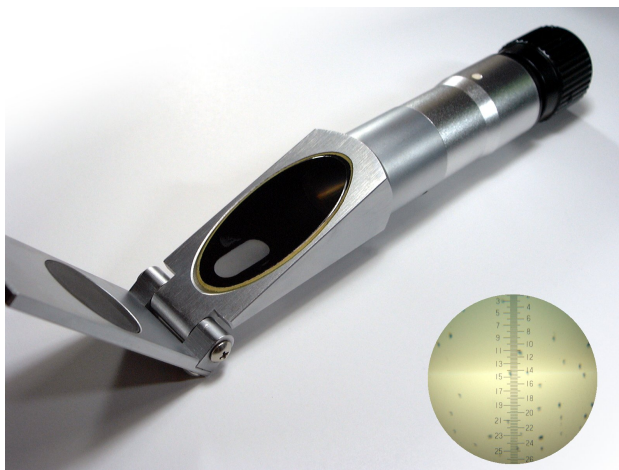


Figure 1.2: Photo of a Handheld Refractometer used to measure sugar content (Brix level) of fruits. The image includes a view through the eyepiece of the instrument, a small drop of orange juice was put over the measuring prism to take the picture. Image taken from [24]

Acids determination

Acidity in fruits is an important factor in determining maturity. Many fruits have high acidity early in the season, making them unacceptable to consumers even though they meet minimum sugar (Brix) standards. Several fruits have specific Brix/acidity maturity standards required for domestic or international commerce.

The acids proportion may be determined measuring the pH with a pH-meter or by means of acid titration using a formula given by equation 1.1. The titration is normally carried out with sodium hydroxide (NaOH) to a pH end-point of 8.2. Titratable acidity measures the total amount of protons available in the juice and it is expressed in percentage or g/L of the predominant acid. In fruits, such as guava, the predominant acid is citric acid.

$$\%acid = \frac{V(NaOH) \times N \times A.F.}{W_s} \times 100 \quad (1.1)$$

where:

$V(NaOH)$ = NaOH volume in ml.

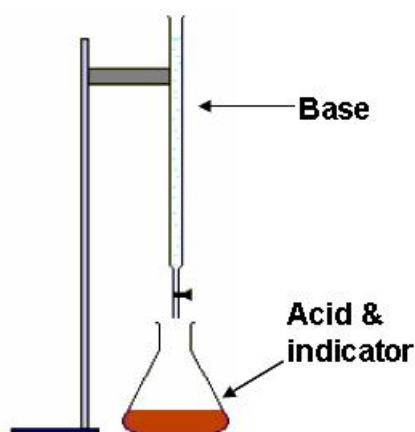


Figure 1.3: Titration apparatus.

$N = NaOH$ normality.

$A.F.$ = Acid Factor.

W_s = Sample weight, in g.

A typical titration begins with a beaker or erlenmeyer flask containing a precisely known volume of the reactant and a small amount of indicator, placed underneath a burette containing the reagent (see Figure 1.3). By controlling the amount of reagent that is added to the reactant, it is possible to detect the point at which the indicator changes color. As long as the indicator has been chosen correctly, this should also be the point where the reactant and reagent neutralise each other, and by reading the scale on the burette the volume of reagent can be measured.

The pH measuring procedure consists in using a potentiometer which uses an electrode whose potential depends on the amount of H^+ ion present in the solution. The pH has no fundamental meaning unit and therefore it is a dimensionless quantity. The pH scale is an inverse logarithmic representation of hydrogen proton (H^+) concentration and measures the activity of hydrogen ions (or their equivalent) in the solution.

Starch content

Starches transform in sugars during the ripening process. A solution of potassium iodide is employed to determine starch content in fruits. Starches in

the presence of this solution turn violet.

Maturity index (I_m)

A minimum value is established for the soluble solids content and a maximum value for the acids. During the ripening process the acids proportion decreases and the sugars increase. The maturity index (I_m) is calculated by the following equation:

$$I_m = \frac{TSS(^{\circ}Brix)}{\%Acid} \quad (1.2)$$

The TSS, acids and TSS-acids ratio are reliable maturity indicators, specially in citric fruits. The greater the I_m , the more ripe the fruit is expected to be [22].

1.2.3 Sensory or Subjective Measurements

Sensory measurements can be classified into two general categories. Consumer acceptance taste tests are frequently conducted in shopping malls, supermarkets, and other areas having large numbers of consumers. The purpose of these tests is to obtain a general profile of consumer acceptance or rejection of the product. Since consumers are not trained panelists, the results of the tests are essentially qualitative. The information gathered provides consumer reaction, which includes numerous characteristics of which texture is but one factor. The test results are not normally very helpful in identifying methods to improve the product [25].

The second category of measurements includes those tests conducted by professionals with experience in sensory evaluation techniques. The panelists are trained to detect, with a high degree of replication, specific food characteristics such as tenderness/toughness, flavor, juiciness, brittleness/softness, sponginess, odor, etc. In highly controlled sensory evaluation laboratories, the panelists are periodically blind tested to evaluate scientific standards. A sensory panel commonly consists of 6 to 12 people who can evaluate up to 10 characteristics on a 1 to 10 scale in one session of 1 to 3 hours. There is wide variation between people in their ability to detect individual food characteristics. Results from the sensory evaluation tests are often correlated with those obtained from instrumental or objective measurement methods as a means to determine the use of the non-sensory tests.

1.3 Non-destructive testing (NDT) methods

Various NDT methods have been applied to fruit-quality testing in the last 25 years with varying degrees of success. Several methods have proved to be accurate enough and otherwise appropriate for use in automatic sorting.

1.3.1 Electromagnetic technologies

The electromagnetic spectrum encompasses, from longest to shortest wavelengths, radiowave, microwave, ultraviolet, visible light, infrared, Xray and gamma-ray radiation. Optical properties indicate the response of matter to visible light wavelengths (400–700 nm, sometimes given as 380–770 nm), and usage is often extended to include ultraviolet (UV, 4–400 nm) and near infrared (NIR, 700 or 770 to 2500 nm). For convenience, the term light will be used loosely to encompass the UV, visible and NIR ranges in the following sections unless otherwise qualified.

Optical properties

Appearance is a primary factor in quality judgments of fruits and vegetables. Light reflected from the product carries information used by inspectors and consumers to judge several aspects of quality; however, human vision is limited to a small region of the spectrum. Colorimeters measure light in terms of a tristimulus color space that relates to human vision; they are restricted to the visible light region. Some quality features respond to wavelengths in regions outside the visible spectrum. Spectrometers and spectrophotometers measure wavelengths in the UV, visible and NIR spectral regions; instruments are optimized for a particular wavelength range. Optical properties are based on reflectance, transmittance, absorbance, or scatter of light by the product. When a fruit or vegetable is exposed to light, about 4% of the incident light is reflected at the outer surface, causing specular reflectance or gloss, and the remaining 96% of incident energy is transmitted through the surface into the cellular structure of the product where it is scattered by the small interfaces within the tissue or absorbed by cellular constituents [26] (Figure 1.4). The complex physical structure of tissues creates an optically dense product that is difficult to penetrate and alters the pathlength traveled by the light so that the amount of tissue interrogated is not known with certainty. Most light energy penetrates only a very short distance and exits

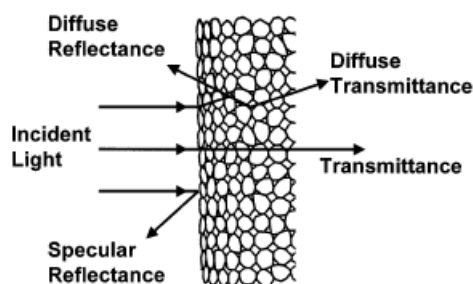


Figure 1.4: Incident light on a fruit or vegetable results in specular reflectance (gloss), diffuse reflectance from features at depths to about 5 mm (body reflectance or interactance), diffuse transmittance, or absorbance. Color results from very shallow diffuse reflectance.

near the point of entry; this is the basis for color.

Color is the basis for sorting many products into commercial grades, but concentration of pigments or other specific constituents might provide a better quality index [27]. Color relates more directly to consumer perception of appearance, pigment concentration may be more directly related to maturity, and concentration of certain other constituents relates more closely to flavor.

Color of an object can be described by several color coordinate systems. Some of the most popular systems are RGB (red, green and blue), which is used in color video monitors, Hunter L a b, CIE (Commission Internationale de l'Eclairage) $L^* a^* b^*$, CIE XYZ, CIE $L^* u^* v^*$, CIE Yxy, and CIE LCH. These differ in the symmetry of the color space and in the coordinate system used to define points within that space. Of greatest importance to instrumental measurement are the tristimulus methods of the CIE and the similar Hunter system. According to CIE concepts, the human eye has three color receptors red, green and blue and all colors are combinations of those. The most commonly used notations are the CIE Yxy color space devised in 1931, the Hunter L a b developed in 1948 for photoelectric measurement, and the CIE $L^* a^* b^*$ color space (Figure 1.5) devised in 1976 to provide more uniform color differences in relation to human perception of differences. Color is measured by colorimeters in which the sensors are filtered to respond similarly to the human eye. Automated color sorting is commercially used on packing lines for apples, peaches and several other horticultural commodities.

Chemical bonds absorb light energy at specific wavelengths, so some com-

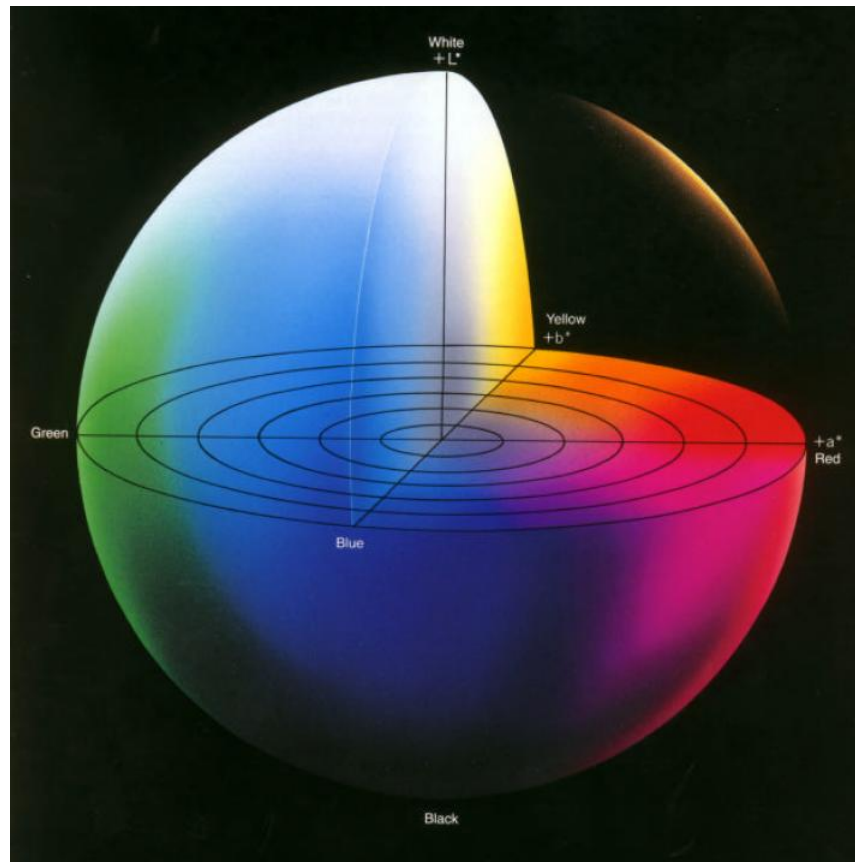


Figure 1.5: CIE $L^*a^*b^*$ color space. L^* indicates lightness, from *white* = 100 to *black* = 0; a^* and b^* are XY color coordinates indicating color directions; a^* is the redgreen axis, b^* is the yellow and blue axis; the center is achromatic gray. Hue is location around the circumference and saturation is distance from center. (Minolta [28]).

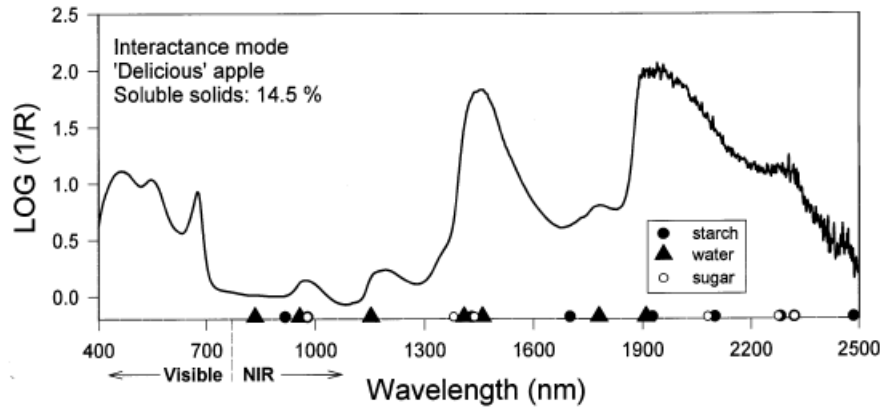


Figure 1.6: Visible and near infrared interactance spectrum of “Delicious apple”. Strongest absorption wavelengths of water, starch and sugar are indicated on the X axis.

positional information can be determined from spectra measured by spectrophotometers or spectrometers. Within the visible wavelength range, the major absorbers are the pigments: chlorophylls, carotenoids, anthocyanins and other colored compounds. Water, carbohydrates, fats and proteins have absorption bands in the NIR region.

Currently multiwavelength or whole-spectra analytical methods are being developed for non-destructive determination of soluble solids, acids, starches and ripeness (Figure 1.6). Starch or soluble solids (SS) content can be determined in intact fruit (apple, citrus, kiwifruit, mango, melons, onion, peach, potato and tomato) with $R^2 \approx 0.93$ and SEC (standard error of calibration) $\approx 0.5\%$ SS [30, 31].

Multi- or hyperspectral cameras permit rapid acquisition of images at many wavelengths. Imaging at fewer than ten wavelengths is generally termed multispectral, and more than ten termed hyperspectral. The resulting dataset can be visualized as a cube with the X and Y dimensions being the length and width of the image (in pixels) and the Z dimension being spectral wavelengths; each datapoint is an intensity value. Alternatively, the dataset could be envisioned as a stack of single wavelength pictures of the object, with as many pictures as the number of wavelengths used. Such imaging provides information about the spatial distribution of constituents (pigments, sugars, moisture, etc.) near the product’s surface.

Differences in images taken at specific wavelengths—multispectral or hy-

perspectral imaging—and computerized image processing techniques are being used to automate detection and classification of many defects on-line. Such sorters are presently in the advanced commercial testing stage.

In addition to imaging technologies, the major advances in spectral analysis in recent years have been in statistical methods. Early analysis used multiple linear regression of raw, first difference, or second difference spectra [32]. Later methods used various forms of data reduction such as principal component or partial least squares coupled with multiple regression. Present investigations focus on artificial neural networks and wavelets for data reduction.

Regardless of the statistical methods, it is critical that the underlying relationship between the measurement and the quality attribute be valid and robust.

Fluorescence and delayed light emission

Fluorescence results from excitation of a molecule by high energy light (short wavelength) and its subsequent instantaneous relaxation with the emission of lower energy light (longer wavelength). Many agricultural materials fluoresce; however, nearly all horticultural applications of fluorescence involve chlorophyll. Delayed light emission (DLE) is a related phenomenon in which chlorophyll is excited by back reactions of photosynthetic intermediates and then relaxes as in fluorescence. Peak excitations of chlorophyll are induced by wavelengths around 420 nm (blue) or around 680 nm (red). The peak emission occurs at 690 nm with a small peak between 720 and 750 nm.

Fluorescence or DLE imaging should enable visualization of the spatial distribution of stress responses before visible symptoms develop [33]. This should be of considerable interest in physiological studies of chilling injury and similar stress responses on fruits and vegetables.

X-ray

X-ray has been explored for inspecting the interior of agricultural commodities. The intensity of energy exiting the product is dependent upon the incident energy, absorption coefficient, density of the product and sample thickness. Due to the high moisture content in fruits and vegetables, water dominates X-ray absorption.

Anatomical and physiological changes within the tissue of fruits and vegetables such as cell breakdown, water distribution and binding, decay and insect infestation have negative effects on quality. Internal disorders cited in grade standards that should be detectable by X-ray include: cork spot, bitter pit, watercore and brown core for apple; blossom end decline, membranous stain, black rot, seed germination and freeze damage for citrus; and hollow heart, bruises and perhaps black heart for potato. Changes in the density of the internal tissue or distribution of water are usually associated with these defects, chilling injury and insect bodies or feeding.

Researchers have investigated X-ray techniques for detecting watercore in apple, split pit in peach, the presence of pits in processed olive and cherry, freeze damage in citrus, bruises, and the presence or feeding of insects on numerous commodities [34].

Magnetic resonance and magnetic resonance imaging (MRI)

Magnetic resonance imaging (MRI) is a noninvasive technique with high potential for visualisation of both water distribution and anatomical interior of food [35]. In ^1H MRI, the specimen is investigated in a magnet equipped with gradient coils, which allows a shaping of the magnetic field in a controlled manner. ^1H MRI proton spins are excited by radio frequency (RF) pulses. Immediately following the RF pulses, the spin relaxation starts. This process is controlled by factors like molecular (primarily water) motion, dephasing due to interactions between molecules (spinspin interactions) and main field inhomogeneities. In short, the first factor determines the T_1 , whereas the first and second determine T_2 and the second and third the T_2^* characteristic relaxation times. In this way, it is possible to image various characteristics of the proton distribution in the specimen, which in biological samples basically corresponds to the water distribution. The intensities of the pixels in the resulting image can be modulated according to the individual MRI parameters.

Currently, MR and MRI are not practical for routine quality testing. MR equipment is expensive and difficult to operate; but, like all technologies, it is becoming cheaper, faster and more feasible for research and specialized applications. MR techniques have great potential for evaluating the internal quality of fruits and vegetables [36].

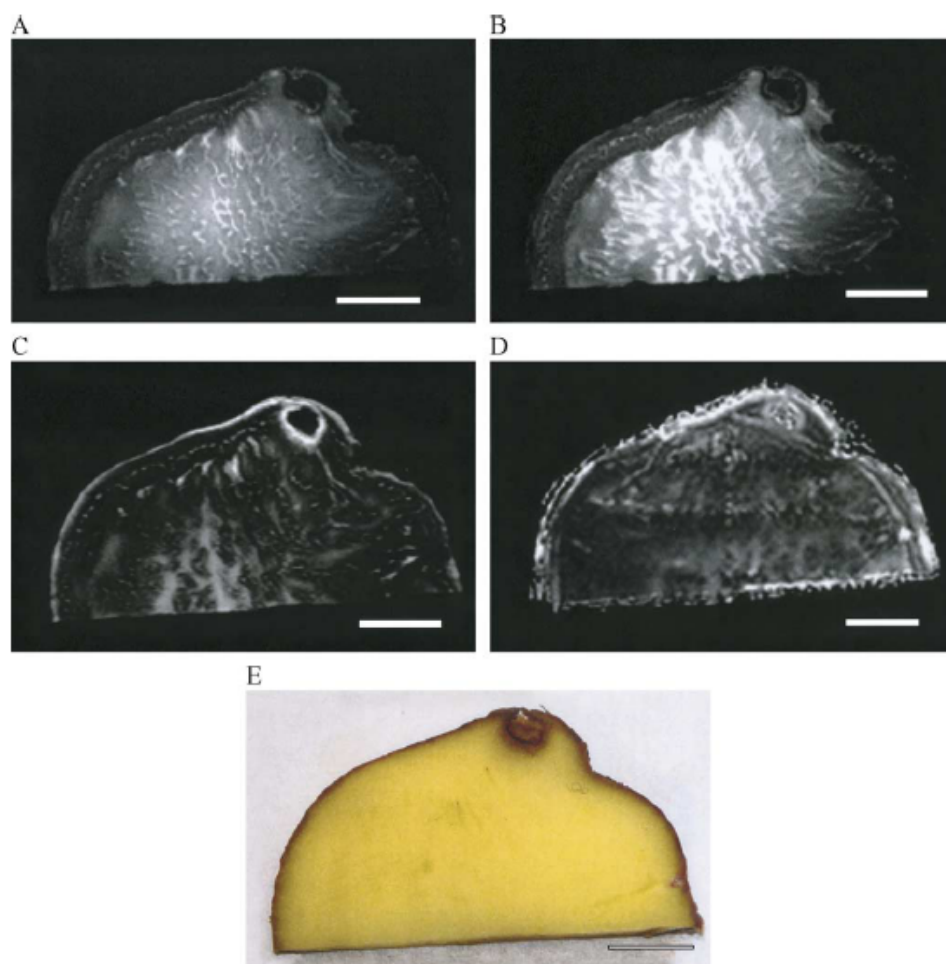


Figure 1.7: (A) Proton-, (B) T₁- and (C) a T₂-weighted images, (D) T₂ map and (E) digital photograph of a bruised potato (Bar = 1 cm). (A.K. Thybo et al. [36]).

1.3.2 Mechanical technologies

Impact

There are various forms of impact test in which the force/time or force/frequency spectrum is recorded as the fruit is dropped onto a force transducer or as the transducer impacts the fruit. A number of impact parameters have been related to firmness: peak force, ratio of peak force to time-to-peak (or time squared), coefficient of restitution, contact time and frequency spectrum. Bajema et al. [37] developed an impact tester for research on bruise resistance. Delwiche et al. [38] developed a single-lane firmness sorting system with a rate of 5 fruit s^{-1} for sorting pear and peach. Delwiche and Sari [39] and Sugiyama et al. [40] developed probe impact sensors that use peak force or coefficient of restitution for firmness measurement.

Sonic and ultrasonic vibration

Sonic (or acoustic) vibrations encompass the audible frequencies between about 20 Hz and ≈ 15 kHz; ultrasonic vibrations are above the audible frequency range (>20 kHz).

Sonic and ultrasonic waves can be transmitted, reflected, refracted or diffracted as they interact with the material. Wave propagation velocity, attenuation and reflection are the important parameters used to evaluate the tissue properties of horticultural commodities.

When an object is excited at sonic frequencies, it vibrates. At particular frequencies it will vibrate more vigorously, causing amplitude peaks; such a condition is referred to as resonance. Resonant frequencies are related to elasticity, internal friction or damping, shape, size and density. The firmer the flesh, the higher the resonant frequency for products of the same size and shape. The traditional watermelon ripeness test is based on the acoustic principle, where one thumps the melon and listens to the pitch (frequency) of the resonance. The sonic vibration method is truly non-destructive and is suitable for rapid firmness measurement. Sonic measurement generally represents the mechanical properties of the entire fruit, unlike puncture or compression which samples localized tissues.

Stiffness coefficients incorporating resonant frequency and mass can compensate for size differences; however, shape also influences sonic firmness measurements [41]. Sonic measurement is an excellent means for following changes in individuals over time in research applications and is suitable for

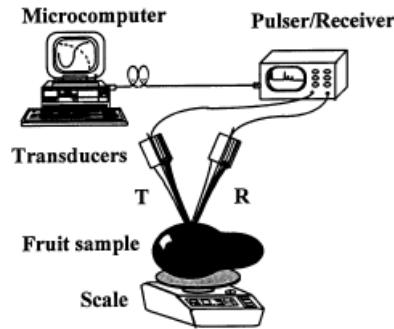


Figure 1.8: Visualisation of the experimental setup. (Mizrach et al. [1]).

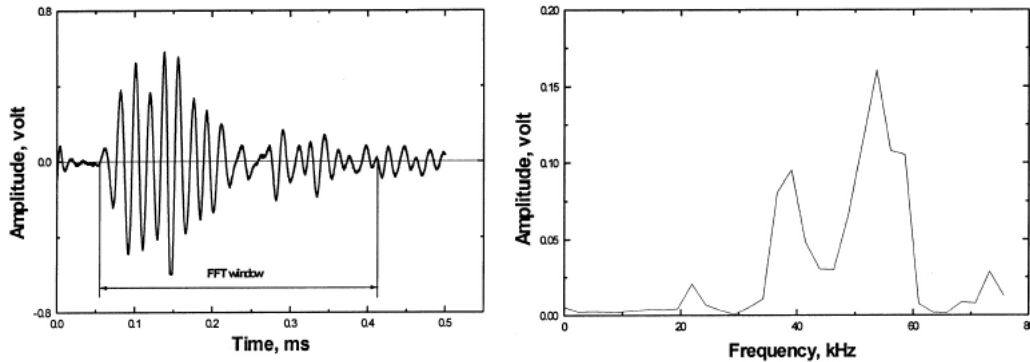


Figure 1.9: Visualisation of input ultrasonic waveform and the fourier transform of that waveform. (Mizrach et al. [1]).

determining average firmness of lots of fruit, but has not always proved capable of predicting the Magness–Taylor firmness of individual fruit [42, 43].

Mizrach et al. [1] conducted a study, based on their previous work on ultrasonics and fruit, to use the result of ultrasonic excitation to calculate the properties of fruit including: firmness, sugar content, storage time, mass and acidity (Figure 1.8). The process used frequency analysis to evaluate the firmness and from that, estimate other properties and then compared these results with trusted destructive methods. They claim that, while the results are not especially accurate, overall reasonable predictions can be made showing that the method is valid.

Ultrasonic waves can be transmitted, reflected, refracted or diffracted as

they interact with the material. Wave propagation velocity, attenuation and reflection are the important ultrasonic parameters used to evaluate the tissue properties of horticultural commodities. However, because of the structure and air spaces in fruits and vegetables, it is difficult to transmit sufficient ultrasonic energy through them to obtain useful measurements.

1.3.3 Electrochemical technologies

The concentration of volatiles within a fruit or vegetable increases as it ripens and their release to the surrounding atmosphere is responsible for the product's pleasing aroma. Aromatic and non-aromatic volatiles are released, including ethylene, ethyl esters, acetaldehyde, ethanol and acetate esters. The electrical conductivity of semiconductor gas detectors, based on different polymers and metal oxides, decreases on exposure to volatiles. Although the detectors are not specific for particular volatiles, each type is generally sensitive to a particular class of compounds. A battery of several detectors can produce a "fingerprint" that may indicate maturity or presence of some disorders. The electronic nose concept (Brezmes et al. [44]) has been tested on peaches, nectarines, apples, and pears. Further research is needed to explore the selection of semiconductors and to relate the fingerprints to quality categories.

1.4 Machine vision and fruit sorting

Machine vision (MV) is the application of computer vision to industry and manufacturing. Machine Vision is a subfield of engineering that encompasses computer science, optics, mechanical engineering, and industrial automation. One of the most common applications of Machine Vision is the inspection of manufactured goods such as semiconductor chips, automobiles, food and pharmaceuticals.

Machine vision systems are programmed to perform narrowly defined tasks such as counting objects on a conveyor and searching for surface defects. Manufacturers favor machine vision systems for visual inspections that require high-speed, high-magnification, 24-hour operation, and/or repeatability of measurements.

Computers do not 'see' in the same way that human beings are able to. Cameras are not equivalent to human optics and while people can rely on in-

ference systems and assumptions, computing devices must 'see' by examining individual pixels of images, processing them and attempting to develop conclusions with the assistance of knowledge bases and features such as Pattern recognition engines.

1.4.1 Components of a machine vision system

A typical machine vision system will consist of several among the following components (see Figure 1.10):

1. One or more digital or analog camera (black-and-white or colour) with suitable optics for acquiring images.
2. Camera interface for digitizing images (widely known as a "frame grabber").
3. A processor (often a PC or embedded processor, such as a DSP).
4. Input/Output hardware (e.g. digital I/O) or communication links (e.g. network connection or RS-232) to report results.
5. Lenses to focus the desired field of view onto the image sensor.
6. Suitable, often very specialized, light sources (LED illuminators, fluorescent or halogen lamps etc.).
7. A program to process images and detect relevant features.
8. A synchronizing sensor for part detection (often an optical or magnetic sensor) to trigger image acquisition and processing.
9. Some form of actuators used to sort or reject defective parts.

The sync sensor determines when a part (often moving on a conveyor) is in position to be inspected. The sensor triggers the camera to take a picture of the part as it passes beneath the camera and often synchronizes a lighting pulse to freeze a sharp image. The lighting used to illuminate the part is designed to highlight features of interest and obscure or minimize the appearance of features that are not of interest (such as shadows or reflections). LED panels of suitable sizes and arrangement are often used to this purpose.

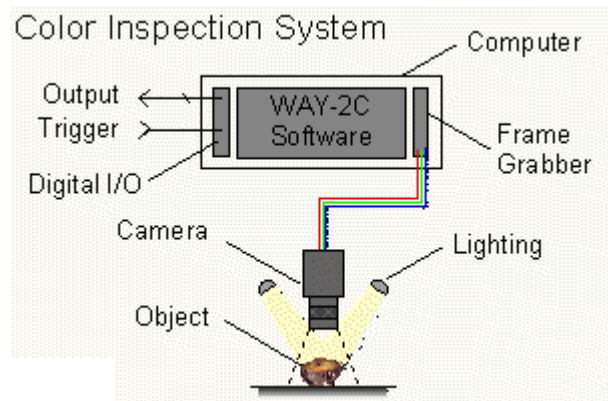


Figure 1.10: Components of machine vision system. (McConnell et al. [2]).

The camera's image is captured by the framegrabber. A framegrabber is a digitizing device that converts the output of the camera to digital format and places the image in computer memory so that it may be processed by the machine vision software.

The software will typically take several steps to process an image. Often the image is first manipulated to reduce noise or to convert many shades of gray to a simple combination of black and white (binarization). Following the initial simplification, the software will count, measure, and/or identify objects, dimensions, defects or other features in the image. As a final step, the software passes or fails the part according to programmed criteria. If a part fails, the software may signal a mechanical device to reject the part; alternately, the system may stop the production line and warn a human worker to fix the problem that caused the failure.

Though most machine vision systems rely on black-and-white cameras, the use of color cameras is becoming more common. It is also increasingly common for MV systems to include digital camera equipment for direct connection rather than a camera and separate framegrabber, thus reducing signal degradation.

1.4.2 Image acquisition

Figure 1.11 shows the three principal sensor arrangements used to transform illumination energy into digital images. The idea is simple: Incoming energy is transformed into a voltage by the combination of input electrical power

and sensor material that is responsive to the particular type of energy being detected. The output voltage waveform is the response of the sensor(s), and a digital quantity is obtained from each sensor by digitizing its response.

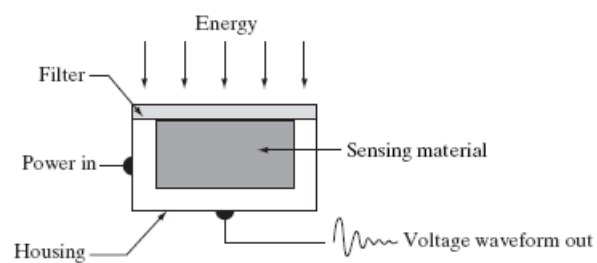
Individual sensors arranged in the form of a 2-D array are shown in Figure 1.11(c). This is also the predominant arrangement found in digital cameras. A typical sensor for these cameras is a CCD array, which can be manufactured with a broad range of sensing properties and can be packaged in rugged arrays of 4000×4000 elements or more. CCD sensors are used widely in digital cameras and other light sensing instruments. The response of each sensor is proportional to the integral of the light energy projected onto the surface of the sensor. Noise reduction is achieved by letting the sensor integrate the input light signal over minutes or even hours. Since the sensor array shown in Figure 1.12(c) is two dimensional, its key advantage is that a complete image can be obtained by focusing the energy pattern onto the surface of the array [3].

The principal manner in which array sensors are used is shown in Figure 1.12. This figure shows the energy from an illumination source being reflected from a scene element. The first function performed by the imaging system shown in Figure 1.12(c) is to collect the incoming energy and focus it onto an image plane. If the illumination is light, the front end of the imaging system is a lens, which projects the viewed scene onto the lens focal plane, as Figure 1.12(d) shows. The sensor array, which is coincident with the focal plane, produces outputs proportional to the integral of the light received at each sensor. Digital and analog circuitry sweep these outputs and convert them to a video signal, which is then digitized by another section of the imaging system. The output is a digital image, as shown diagrammatically in Figure 1.12(e).

1.4.3 Fruit sorting

For a long time, the agro-industry has attempted to automate fruit selection in order to decrease production costs and increase the quality of the production. In the packing lines, where most external quality attributes are currently inspected visually, machine vision provides a means of performing this task automatically [46].

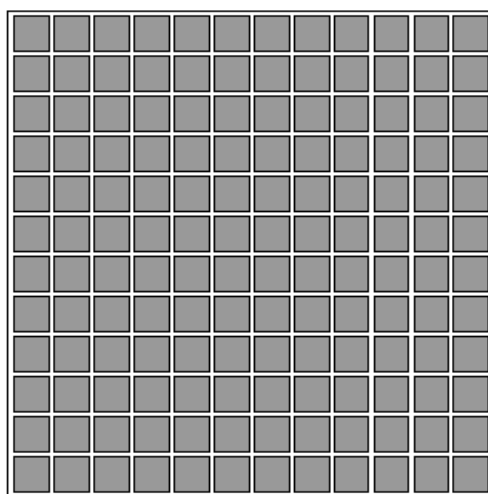
It is evident that routine fruit sorting techniques have to be of non-destructive nature. Optic determinations, in particular, are expected to ensure fast measurements with limited sample preparation; this feature fits



(a) Single imaging sensor.



(b) Line sensor.



(c) Array sensor.

Figure 1.11: The three principal sensor arrangements used to transform illumination energy into digital images. (Gonzalez and Woods [3]).

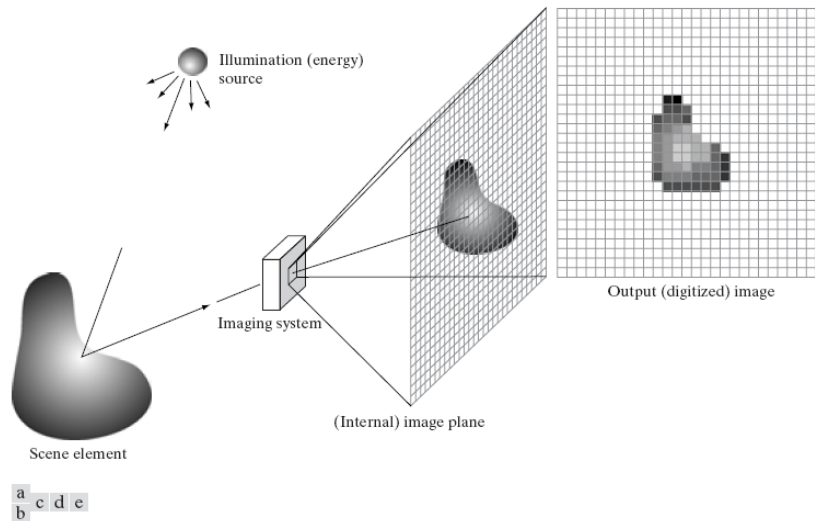


Figure 1.12: An example of the digital image acquisition process. (a) Energy (*illumination*) source. (b) An element of a scene. (c) Imaging system. (d) Projection of the scene onto the image plane. (e) Digitized image. (Gonzalez and Woods [3]).

with the requirement of online process control and produces grading systems.

Several classification methods have been explored consisting in assessing fruit quality as well as bruise detection. Feng et al. [4] built a color image processing based vision system for sorting of Fuji apples (see Figure 1.13). The color ratio of the fruit image is the key feature in the quality grading of the apples and a classic bayes classifier¹ is responsible for the classification. The experimental results showed that the performance of the system was stable and satisfying. Di Natale et al. [47] applied the computer screen photoassisted technique (CSPT), with low-cost electronics, to multispectral imaging of apricot fruits in order to sort the fruits according to their quality, or better to sort fruits treated after harvest.

Pla et al. [5] were able to develop a system using low-cost standard hardware meeting requirements of speed and accuracy of measurements (see Figure 1.14). This system is able to control up to 10 conveyor belts classifying

¹For more information on bayes classifiers see: Rish, Irina. (2001). "An empirical study of the naive Bayes classifier". IJCAI 2001 Workshop on Empirical Methods in Artificial Intelligence. (available online: <http://www.research.ibm.com/people/r/rish/papers/RC22230.pdf>)

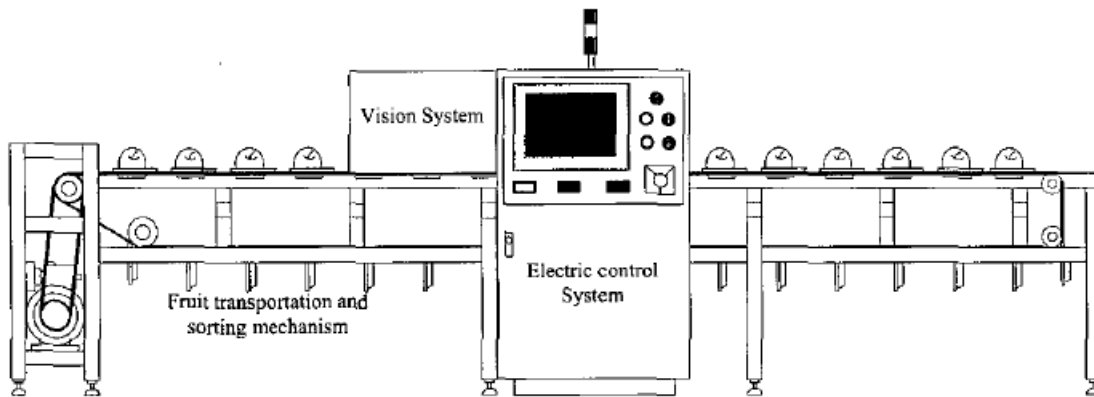


Figure 1.13: Intelligent fruit sorting system. (Feng et al. [4]).

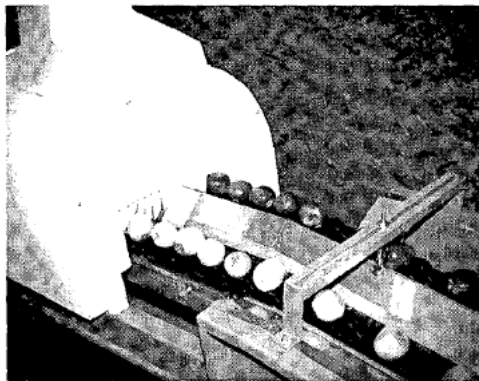


Figure 1.14: Illumination chamber. (Pla et al. [5]).

fruits according to their weight, size and color, and distributing the fruits in different outputs at a maximum speed of 15 fruits per second per belt approximately.

Different fruit sorting techniques based on optical properties and image analysis have been researched as well as the classification methods, including k-means, bayes, neural-networks and vector-support machines. There is no industry standard to date, the trend in the field appears to be high-performance systems using low-cost standard architectures.

1.5 Digital image processing

Interest in digital image processing methods stems from two principal application areas: improvement of pictorial information for human interpretation; and processing of image data for storage, transmission, and representation for autonomous machine perception.

1.5.1 Digital image and basic concepts

An image may be defined as a two-dimensional function, $f(x, y)$, where x and y are spatial (plane) coordinates, and the amplitude of f at any pair of coordinates (x, y) is called the intensity or gray level of the image at that point. When x , y , and the amplitude values of f are all finite, discrete quantities, we call the image a *digital image* [3]. The field of digital image processing refers to processing digital images by means of a digital computer. Note that a digital image is composed of a finite number of elements, each of which has a particular location and value. These elements are referred to as *picture elements*, *image elements*, *pels*, and *pixels*. *Pixel* is the term most widely used to denote the elements of a digital image.

In order for a computer to process an image, it has to be described as a series of numbers, each of finite precision [6]. The digitization of $f(x, y)$ is called:

1. *Image sampling* when it refers to spatial coordinates (x, y) and
2. *Quantization* when it refers to the amplitude of $f(x, y)$.

The result of sampling and quantization is a matrix of real numbers. A way of representing the image is to assume that an image $f(x, y)$ is sampled so that the resulting digital image has M rows and N columns and G number of discrete gray-levels allowed for each pixel. The values of the coordinates (x, y) now become discrete quantities. For notational clarity and convenience, integer values are used for these discrete coordinates. Thus, the values of the coordinates at the origin are $(x, y) = (0, 0)$. Figure 1.15 shows the coordinate convention used.

The notation introduced in the preceding paragraph allows us to write the complete $M \times N$ digital image in the following compact matrix form:

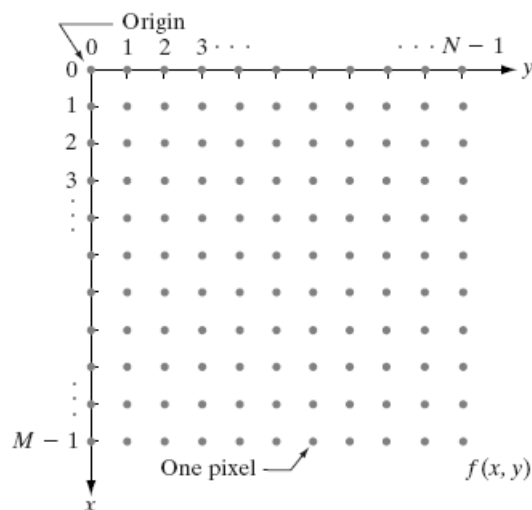


Figure 1.15: Coordinate convention used to represent digital images. (Gonzalez and Woods [3]).

$$f(x, y) = \begin{bmatrix} f(0, 0) & f(0, 1) & \cdots & f(0, N-1) \\ f(1, 0) & f(1, 1) & \cdots & f(1, N-1) \\ \vdots & \vdots & & \vdots \\ f(M-1, 0) & f(M-1, 1) & \cdots & f(M-1, N-1) \end{bmatrix} \quad (1.3)$$

In digital image processing the quantities M , N and G are usually powers of two, thus:

$$N = 2^n \quad M = 2^m \quad G = 2^k$$

1.5.2 Spatial and gray-level resolution

Sampling is the principal factor determining the spatial resolution of an image. Basically, spatial resolution is the smallest discernible detail in an image. Gray-level resolution similarly refers to the smallest discernible change in gray level. There is considerable discretion regarding the number of samples used to generate a digital image, but this is not true for the number of gray levels [3]. Due to hardware considerations, the number of gray levels is usually an integer power of 2, as mentioned previously.

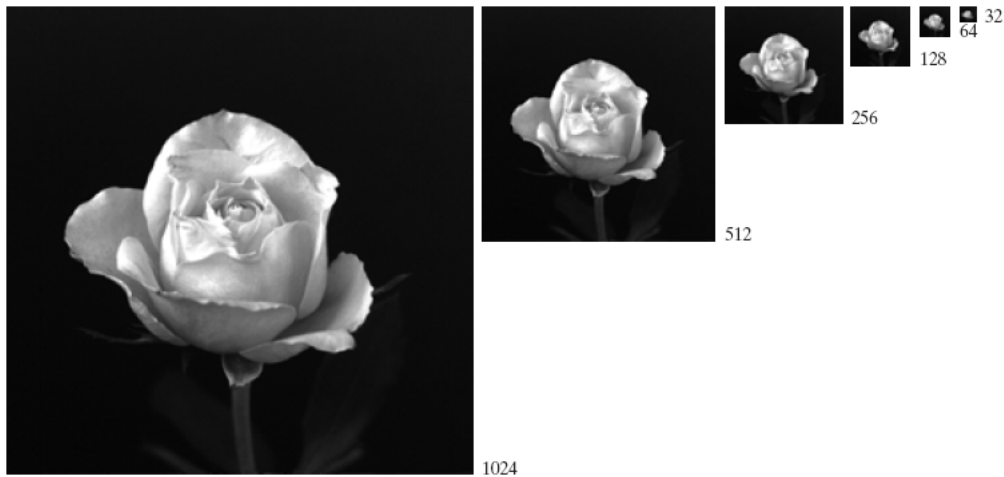


Figure 1.16: A 1024×1024 , 8-bit image subsampled down to size 32×32 pixels. The number of allowable gray levels was kept at 256. (Gonzalez and Woods [3]).

To illustrate these concepts two examples where spatial resolution (*sub-sampling* Figure 1.16) and gray-level resolution (*resampling* Figure 1.17) are modified are shown. Figure 1.16 shows an image of size 1024×1024 pixels whose gray levels are represented by 8 bits. These are the effects of varying the number of samples in a digital image. In Figure 1.17, the number of samples is kept constant and the number of gray levels is reduced from 256 to 2, in integer powers of 2. The resulting effects of varying the number of gray levels in a digital image are evident.

In conclusion the bigger these parameters the closer the digitized image approximates the original image, but the storage and processing times increase exponentially.

1.5.3 Basic Relationships Between Pixels

Neighbors of a Pixel

A pixel p at coordinates (x, y) has four horizontal and vertical neighbors whose coordinates are given by

$$(x + 1, y), (x - 1, y), (x, y + 1), (x, y - 1)$$

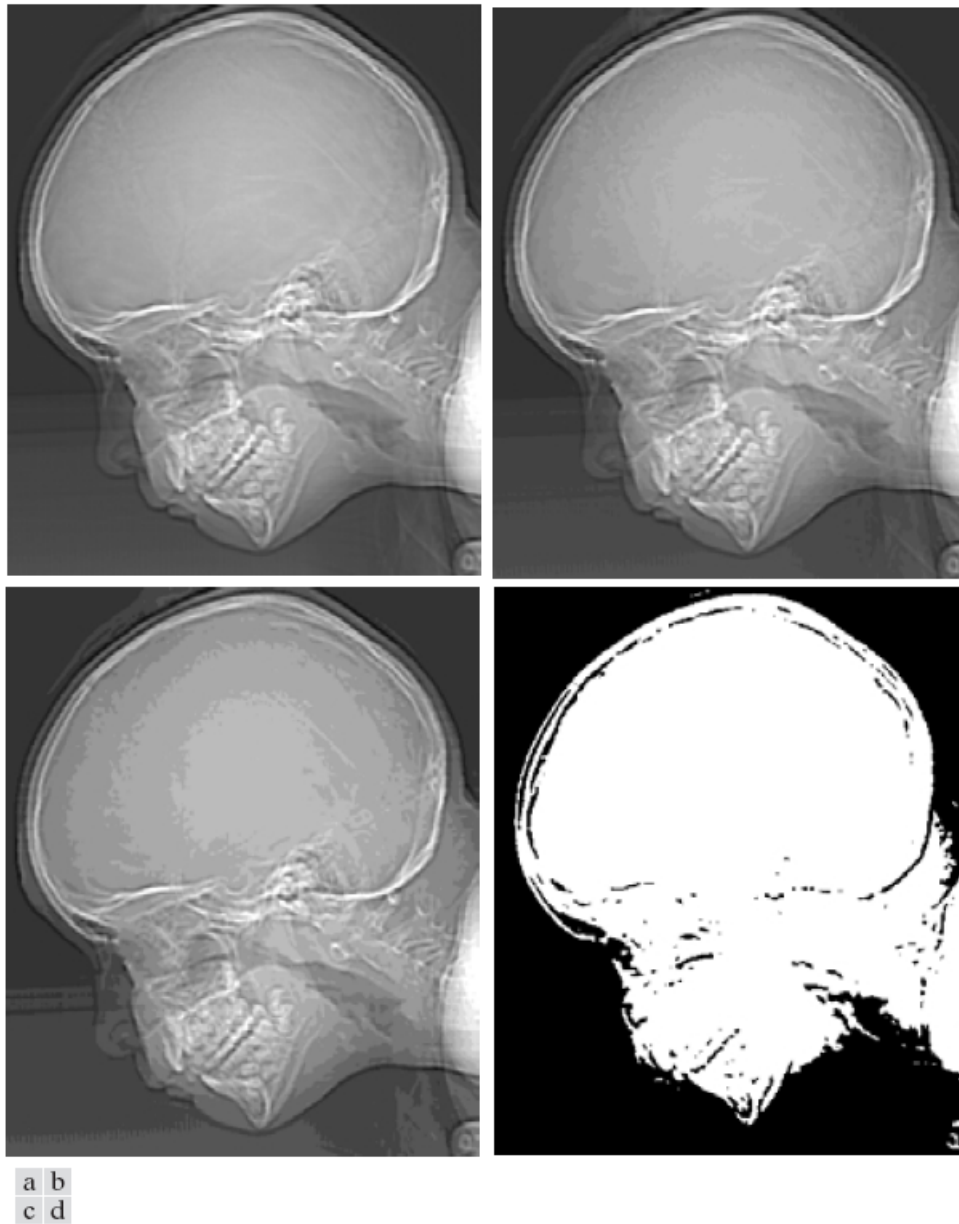


Figure 1.17: (a) 452×374 , 256-level image. (b)-(d) Image displayed in 32, 16, and 2 gray levels, while keeping the spatial resolution constant. (Gonzalez and Woods [3]).

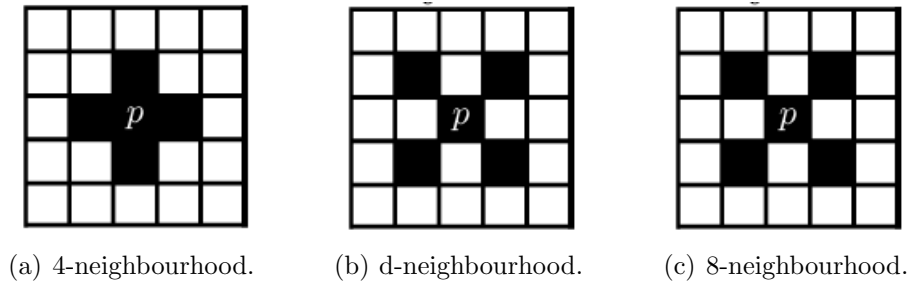


Figure 1.18: Pixel neighbourhoods. (Cattin [6]).

This set of pixels, called the *4-neighbors* of p , is denoted by $N_4(p)$ (Figure 1.18(a)). Each pixel is a unit distance from (x, y) , and some of the neighbors of p lie outside the digital image if (x, y) is on the border of the image.

The four *diagonal* neighbors of p have coordinates

$$(x + 1, y + 1), (x + 1, y - 1), (x - 1, y + 1), (x - 1, y - 1)$$

and are denoted by $N_D(p)$ (Figure 1.18(b)). These points, together with the *4-neighbors*, are called the *8-neighbours* of p , denoted by $N_8(p)$ (Figure 1.18(c)). As before, some of the points in $N_D(p)$ and $N_8(p)$ fall outside the image if (x, y) is on the border of the image.

Connectivity

The connectivity is important to establish boundaries around objects and to extract connected components in an image. To establish if two pixels are connected, it must be determined if they are neighbors (e.g. $N_4(p), N_8(p), \dots$) and if their gray levels satisfy a specified criterion of similarity (say, if their gray levels are equal). For instance, in a binary image with values 0 and 1, two pixels may be *4-neighbors*, but they are said to be connected only if they have the same value.

Let V be the set of gray-level values used to define connectivity; for example in a binary image $V = 1$ or in a gray-scale image $V = 16, 17, \dots, 32$. Two types of connectivity can be defined (see Figure 1.19):

1. *4-connectivity*: Two pixels p and q with values from V are *4-connected* if q is in the set $N_4(p)$.

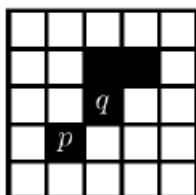


Figure 1.19: The pixels p, q are not connected under 4-*connectivity* but they are under 8-*connectivity*. (Cattin [6]).

2. 8-*connectivity*: Two pixels p and q with values from V are 8-*connected* if q is in the set $N_8(p)$.

1.5.4 Color and color models

The use of color in image processing is motivated by two principal factors. First, color is a powerful descriptor that often simplifies object identification and extraction from a scene. Second, humans can discern thousands of color shades and intensities, compared to about only two dozen shades of gray.

Basically, the colors that humans perceive are determined by the nature of the light reflected from the object. The nature of electromagnetic radiation and the visible spectrum were discussed in section 1.3.1 as well as color coordinate systems (color models).

Color models

The purpose of a color model (also called *color space* or *color system*) is to facilitate the specification of colors in some standard, generally accepted way. In essence, a color model is a specification of a coordinate system and a subspace within that system where each color is represented by a single point.

In digital image processing, the hardware-oriented models most commonly used in practice are the RGB (red,green,blue) model for color monitors and a broad class of color video cameras; the CMY (cyan,magenta,yellow) and CMYK (cyan,magenta,yellow,black) models for color printing; and the HSI (hue,saturation,intensity) model, which corresponds closely with the way humans describe and interpret color. In many color measurement applications the color-model standard is the CIE $L^*a^*b^*$ color space as mentioned in 1.3.1 and with a coordinate representation given in Figure 1.5.

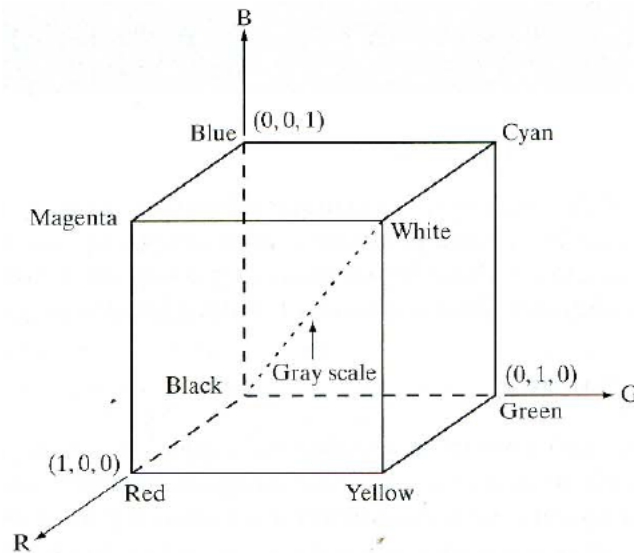


Figure 1.20: Schematic of the RGB color cube. Points along the main diagonal have gray values, from black at the origin to white at point $(1, 1, 1)$. (Gonzalez and Woods [3]).

The RGB color model In the RGB model, each color appears in its primary spectral components of red, green and blue. This model is based on a cartesian coordinate system. The color subspace of interest is the cube shown in Figure 1.20, in which RGB values are at three corners; cyan, magenta and yellow are at three other corners; black is at the origin; and white is at the corner farthest from the origin.

Images represented in the RGB color model consist of three component images, one for each primary color. The number of bits used to represent each pixel in RGB space is called the *pixel depth*. Consider an RGB image in which each of the red, green and blue images is an 8-bit image. Under these conditions each RGB color pixel [that is, a triplet of values (R, G, B)] is said to have a depth of 24 bits (3 image planes times the number of bits per plane).

The CIE LCH color space or color Model There are many CIE colour spaces, more correctly known as models which, serve different purposes. They are all device independent, unlike RGB or CMYK colour spaces which are

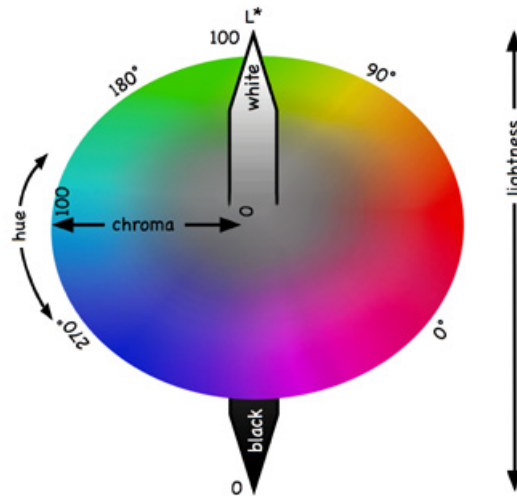


Figure 1.21: The CIE LCH color space. (Graphic Quality Consultancy [48])

related to a specific device (cameras, scanners, presses, etc.) or material type (paper, inks, film emulsions and lighting, etc.). These RGB and CMYK spaces usually do not cover the entire visible colour spectrum or gamut. The CIE also specify lighting conditions.

The LCH model is a little easier to comprehend than the Lab colour space (Figure 1.5), with which it shares several features. Essentially it is in the form of a sphere. There are three axes; L^* , C^* and H° .

The L^* axis represents Lightness (see Figure 1.21). This is vertical; from 0 which has no lightness (i.e. absolute black) at the bottom; through 50 in the middle, to 100 which is maximum lightness (i.e. absolute white) at the top.

If we take a horizontal slice through the centre, we see a colored circle. Around the edge of the circle we see every possible saturated colour or *Hue*. This circular axis is known as H° for Hue. The units are in the form of degrees $^\circ$, ranging from 0° (red) through 90° (yellow), 180° (green), 270° (blue) back to 0° .

The C^* axis represents Chroma or *saturation*. This ranges from 0 at the centre of the circle, which is completely unsaturated (i.e. a neutral grey, black or white) to 100 at the edge of the circle for maximum Chroma or saturation.

1.5.5 Digital image processing techniques

Some of the most important digital image processing techniques used in this work are reviewed; including spatial domain enhancement, morphological processing and image segmentation techniques.

The principal objective of enhancement is to process an image so that the result is more suitable than the original image for a specific application. Image enhancement approaches fall into two broad categories: spatial domain methods and frequency domain methods. The term spatial domain refers to the image plane itself, and approaches in this category are based on direct manipulation of pixels in an image. Frequency domain processing techniques are based on modifying the Fourier transform of an image.

The morphological techniques include pre- or post processing techniques such as morphological filtering, thinning and pruning. The segmentation techniques consist basically in subdividing an image into regions or objects.

Noise reduction through stacking of images

There are various noise reduction techniques available in digital image processing. The technique of image noise reduction by way of *stacking* images is mainly a preprocessing technique, carried out at the image acquisition stage.

The method basically consists in reducing the image noise by taking multiple images of the same object and then *stacking* the images using the computer. By doing this, the noise in the image will tend to *average out* and the object image will add, resulting in a better signal to noise ratio.

For image stacking to work in an ideal fashion, a few things have to be true:

1. The noise in each image frame *must* be truly random.
2. The *object* being imaged *must* be the same in each image.

If the above criteria are not met, the amount of image improvement obtained by stacking images will not be ideal [49].

Consider an image of an object taken by a CCD camera. This image consists of two portions: signal level due solely to noise and signal level due solely to the object being imaged. Ideally we want only the signal that is due to the object. However, it is impossible to determine which part of the total image is due to the object and which part of the total image is due to noise. Given that 2 images of the object are taken under the same

conditions. In each image, the background noise is random; that is, the noise in image number 1 is different from the noise in image number 2. However, the object in both images is the same. By stacking the two images (which in mathematical terms equates to adding the images) we will see that the object looks better, the noise is reduced. This improvement is due to two factors:

- Fact 1: When random signals are added, the resulting total signal of the sum is the same as the sum of the power of the signals. This referred to in the literature as the incoherent gain of a system.
- Fact 2: When identical signals are added, the signal levels add directly. This referred to in the literature as the coherent gain of a system.

A mathematical analysis should show the improvement in the image. Each image is a combination of signal partly due to noise and partly due to the actual object being imaged, thus:

$$Image(total) = image(noise) + image(object)$$

Adding two images or two different exposures of the same object results in:

$$Image_new(total) = \sqrt{image(noise^2 + noise^2)} + 2 \times image(object)$$

To show that there is improvement in the resulting image a brief example is discussed. Given two images taken under the same conditions, suppose the signal in each pixel (due to the object) is a constant value of 20. Also, let's assume (for each of the two images) that the RMS (root mean squared) value of the noise is also 20. So, for this example, the signal to noise ratio for any *one* image is:

$$20 \cdot \log_{10}(signal_value/noise_value) = 20 \cdot \log_{10}(20/20) = 0$$

This means that the signal due to the object is the same as that of the noise; in a real world image the object would be on the threshold of visibility in the image. Now the case of the stacked image. For this case, the summed noise signals produce an RMS level of

$$\sqrt{20 \cdot 20 + 20 \cdot 20} = \sqrt{800} = 28.28$$

Notice that the noise signal went up, however it did not double. Now, looking at the summed signal due to the object, we get

$$2 \cdot 20 = 40$$

In this case the signal does in fact double. So, the signal to noise ratio for this summed image is

$$20 \cdot \log_{10}(40/28.28) = 3.01\text{dB}$$

Thus, by adding the two images, the signal to noise ratio of the image has been increased by 3 dB. In other words the noise in the image has been suppressed by 3 dB. Basically, adding images does increase the noise, but the signal increases more, resulting in the better image.

To illustrate this behavior Table 1.1 shows a typical stacking procedure, the *object* being images consists of three lines of various strengths. Thirty two individual images were generated (using MATLAB [50]). For each of the 32 images, the background noise is identical in level and random from frame to frame. Also, for each of the 32 images, the signal is identical (the signal levels were set so that at least one of them was pretty well *buried* in noise so that the benefit of stacking can be better shown). The results for 4 cases are shown; a single image, and results for 2, 8 and 32 stacked images.

Histogram-based segmentation

As stated before segmentation refers to the process of partitioning a digital image into multiple regions (sets of pixels). The goal of segmentation is to simplify and/or change the representation of an image into something that is more meaningful and easier to analyze. Image segmentation is typically used to locate objects and boundaries (lines, curves, etc.) in images. Several general-purpose algorithms and techniques have been developed for image segmentation [51]. Since there is no general solution to the image segmentation problem, these techniques often have to be combined with domain knowledge in order to effectively solve an image segmentation problem for a problem domain.

Histogram-based methods are very efficient when compared to other image segmentation methods because they typically require only one pass through the pixels. In this technique, a histogram is computed from all of the pixels

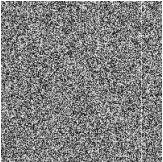
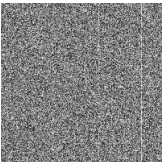
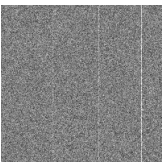
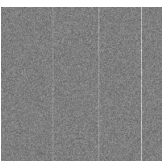
Image	Number of images stacked	Signal to noise ratio of strongest line (dB)	Notes
	1	0	This image shows a <i>salt and pepper</i> characteristic, strongest signal (0db) is barely visible here. The two other signals are at -6 dB and -9 dB, these are totally invisible here. This is a single image, so technically it is not stacked.
	2	+3	The <i>salt and pepper</i> appearance is somewhat muted compared to the previous image. The strongest signal shows better while the two weaker ones (now at -6dB and 0 dB are showing hints of visibility. In this image the noise has essentially been suppressed by 3 dB as compared to a single frame.
	8	+9	Background noise is further smoothed, all three signals are now visible (being at +3, +6 and +9dB level now). In this image the noise has essentially been suppressed by 9 dB as compared to a single frame.
	32	+15	Background noise smoothing out nicely, all signals are easily visible. At this point the signals are not really getting any brighter, they are being "cleaned up" as the noise is suppressed. The weakest signal is now at +6 dB level. In this image the noise has essentially been suppressed by 15 dB as compared to a single frame.

Table 1.1: Stacking Procedure

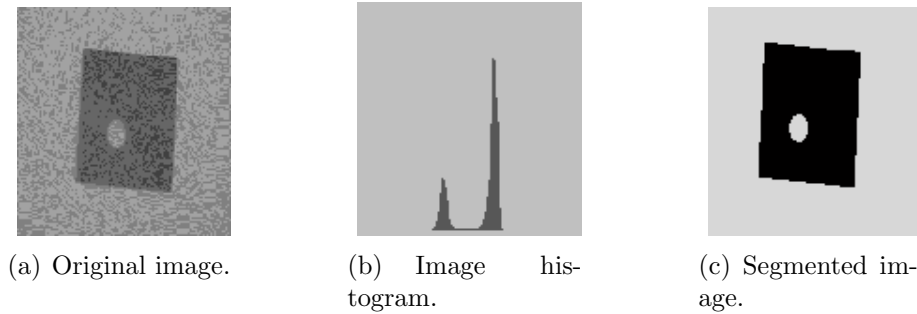


Figure 1.22: Image segmentation via thresholding.

in the image, and the peaks and valleys in the histogram are used to locate the clusters in the image [51]. Color or intensity can be used as the measure.

A refinement of this technique is to recursively apply the histogram-seeking method to clusters in the image in order to divide them into smaller clusters. This is repeated with smaller and smaller clusters until no more clusters are formed.

One disadvantage of the histogram-seeking method is that it may be difficult to identify significant peaks and valleys in the image. This may affect the quality and usefulness of the final solution.

The simplest histogram-based segmentation technique is *thresholding*. Individual pixels in a grayscale image are marked as *object* pixels if their value is greater than some threshold value (assuming an object to be brighter than the background) and as *background* pixels otherwise. Typically, an object pixel is given a value of “1” while a background pixel is given a value of “0”.

The key parameter in thresholding is obviously the choice of the threshold. Several different methods for choosing a threshold exist. The simplest method would be to choose the mean or median value, the rationale being that if the object pixels are brighter than the background, they should also be brighter than the average. In a noiseless image with uniform background and object values, the mean or median will work beautifully as the threshold, however generally speaking, this will not be the case. A more sophisticated approach might be to create a histogram of the image pixel intensities and use the valley point as the threshold (see Figure 1.22). The histogram approach assumes that there is some average value for the background and object pixels, but that the actual pixel values have some variation around these average values.

Erosion

Erosion is one of the two basic operators in the area of mathematical morphology, the other being *dilation*. It is typically applied to binary images, but there are versions that work on grayscale images. The basic effect of the operator on a binary image is to erode away the boundaries of regions of foreground pixels (i.e. white pixels, typically). Thus areas of foreground pixels shrink in size, and holes within those areas become larger.

The erosion operator takes two pieces of data as inputs. The first is the image which is to be eroded. The second is a (usually small) set of coordinate points known as a *structuring element* (also known as a *kernel*). It is this structuring element that determines the precise effect of the erosion on the input image.

The mathematical definition of erosion for *binary* images is as follows:

- Suppose that X is the set of Euclidean coordinates corresponding to the input binary image, and that K is the set of coordinates for the structuring element.
- Let K_x denote the translation of K so that its origin is at x .
- Then the erosion of X by K is simply the set of all points x such that K_x is a subset of X .

As an example of binary erosion, suppose that the structuring element is a 3×3 square, with the origin at its center as shown in Figure 1.23. Note that in this and subsequent diagrams, foreground pixels are represented by 1's and background pixels by 0's.

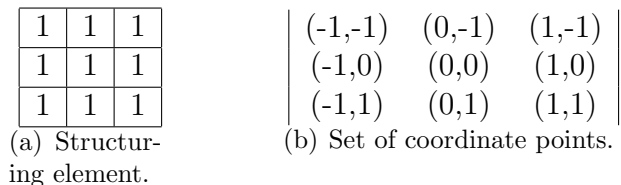


Figure 1.23: A 3×3 structuring element

To compute the erosion of a binary input image by this structuring element, we consider each of the foreground pixels in the input image in turn.

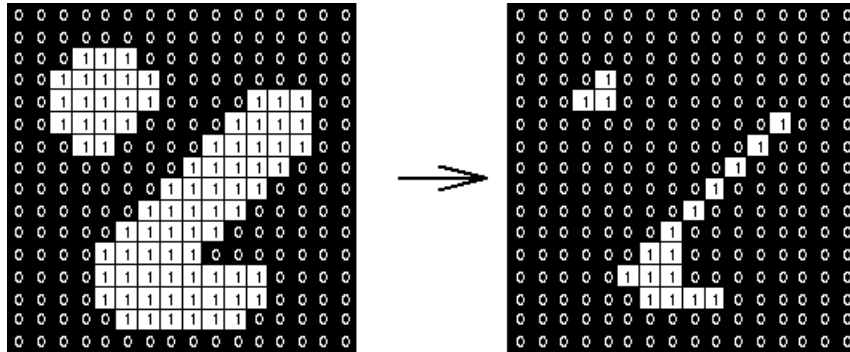


Figure 1.24: Effect of erosion using a 3×3 square structuring element. (Fisher et al. [7])

For each foreground pixel (which we will call the input pixel) we superimpose the structuring element on top of the input image so that the origin of the structuring element coincides with the input pixel coordinates. If for every pixel in the structuring element, the corresponding pixel in the image underneath is a foreground pixel, then the input pixel is left as it is. If any of the corresponding pixels in the image are background, however, the input pixel is also set to background value.

For our example 3×3 structuring element, the effect of this operation is to remove any foreground pixel that is not completely surrounded by other white pixels (assuming *8-connectedness*). Such pixels must lie at the edges of white regions, and so the practical upshot is that foreground regions shrink (and holes inside a region grow).

Erosion is the dual of *dilation*, i.e. eroding foreground pixels is equivalent to dilating the background pixels.

The effect of an erosion using this structuring element on a binary image is shown in Figure 1.24.

1.5.6 Color content-based image classification

Many applications require methods for comparing images based on their overall appearance. Color histograms are a popular solution to this problem because they are easy to compute and effective in characterizing both the global and local distribution of color in an image. In addition, they are robust to translation and rotation about the view axis and change only slowly with

the scale, occlusion and viewing angle.

Since any pixel in the image can be described by three components in a certain color space, a histogram, i.e., the distribution of the number of pixels for each quantized bin, can be defined for each component. Clearly, the more bins a color histogram contains, the more discrimination power it has. However, a histogram with a large number of bins will not only increase the computational cost, but will also be inappropriate for building efficient indexes for image databases.

Color Coherence Vector

In [52] a different way of incorporating spatial information into the color histogram, *color coherence vector* (CCV), was proposed. Each histogram bin is partitioned into two types, i.e., *coherent*, if it belongs to a large uniformly-colored region, or *incoherent*, if it does not. Let α_i denote the number of coherent pixels in the i -th color bin and β_i denote the number of incoherent pixels in an image. Then, the CCV of the image is defined as the vector

$$[(\alpha_1, \beta_1), (\alpha_2, \beta_2), \dots, (\alpha_N, \beta_N)]$$

Note that $[\alpha_1 + \beta_1, \alpha_2 + \beta_2, \dots, \alpha_N + \beta_N]$ is the color histogram of the image.

Two images I, I' can be compared using their CCV's, for example by using the L_1 distance. Let the coherence pairs for the j -th color bucket be (α_j, β_j) in I and (α'_j, β'_j) in I' . Using the L_1 distance to compare CCV's, the j -th bucket's contribution to the distance between I and I' is

$$\Delta_{CCV} = |(\alpha_j - \alpha'_j)| + |(\beta_j - \beta'_j)| \quad (1.4)$$

It follows that CCV's create a finer distinction than color histograms. A given color bucket j can contain the same number of pixels in I as in I' , but these pixels may be entirely incoherent in I and entirely coherent in I' (i.e., $\alpha = \beta' = 0$).

Chapter 2

Experimental design

2.1 Overview

Comparisons between methods found in the available literature show many viable methods for testing fruit ripeness based on optic properties. For the duration of our research we focused on computer vision-based techniques involving low-cost electronics. This approach is sustained under the premise that unparallel technology progress in fields as consumer electronics, produced a number of low-cost advanced optical equipments such as digital scanners, video cameras, and screens that possess unexpected properties that could be usefully exploited in routine analysis. Special interest attracted the work from Filippini and Lundström [53] who showed that a combination of computer monitor and an inexpensive webcam may be turned into a sort of spectrophotometer instrument. In view of the results obtained by Filippini and Lundström [53] we decided to use a low cost conventional webcam as the image acquisition system.

Based on the principles of a machine vision system (section 1.4) a guava fruit optic inspection system was constructed and the acquisition, pre- and post-processing programs were developed in Matlab [50].

2.2 Proposed system

2.2.1 Materials

The assembled optic inspection system consisted of the image acquisition device, the illumination system, a manipulation base and a computer laptop serving as data storage and image processing device.

Image acquisition device

The image acquisition device used was a *Genius Videocam Messenger 300K* Pixel Internet Video Camera. With an image sensor type VGA (640×480) CMOS image sensor. A maximum color depth of 32 bits and a max AVI frame capture rate of 30 fps.

Illumination system

The illumination system consisted of three conventional edison screw lamps, each with a 8W *daylight* philips energy saver light bulb. These types of lamps are compact fluorescent lamps (CFL) designed to replace incandescent lamps. CFLs were selected because good-quality consumer CFLs typically emit light in the red, green and blue spectra and achieve *white* light with color-rendering indices (CRI) of around 80, although CFLs with a CRI as great as 96 have been developed. (A CRI of 100 represents the most accurate reproduction of all colors; reference sources having a CRI of 100, such as the sun and incandescent tungsten lamps, emit black body radiation.)

A light diffuser system was built as well. Optical diffusers scatter incident light, thereby reducing the so called *bright* spots on the image. The diffuser system was built with opaque acrylic glass (Polymethyl methacrylate), a synthetic polymer methyl methacrylate. Acrylic glass is used in a wide range of fields and applications.

Manipulation base

A general support was built in order to position the acquisition device, the diffuser system and a manipulation base which enabled taking images of all the sides of the fruit. The manipulation base consisted of a small round base, so that the fruit could rest upon it, coupled to a 6Vdc Parallax continuous rotation servo controlled with a Microchip PIC16F819 microcontroller.



Figure 2.1: Parallax continuous rotation servo.

The microcontroller is interfaced with the computer via the RS-232 protocol to perform 90° rotations at the acquisition stage in order to obtain 4 images corresponding to 4 sides of the fruit.

A 2-degrees of freedom support was built for the image acquisition device, so as to locate the fruit within the focal plane of the optic device.

Image processing device

A Dell XPS laptop computer running Microsoft Windows XP Professional edition was used as the image processing device. The system specifications are: 1 GB in RAM, 2.4 GHz intel centrino processor, 80 GB HD. No additional video card was needed since the image acquisition device was interfaced via USB-port.

On board the laptop computer was the technical computing platform, Matlab [50]. Matlab includes excellent signal and image processing and acquisition tools which were used to develop all of the programs needed in the project.

2.2.2 Assembled system

Figure 2.2 shows the assembled optic inspection system. A diagram which allows an easier understanding of the system's operating way is shown in Figure 2.3. The fruit is manually placed on top of the rotating support. The computer acquires the digital images through the usb-port connected

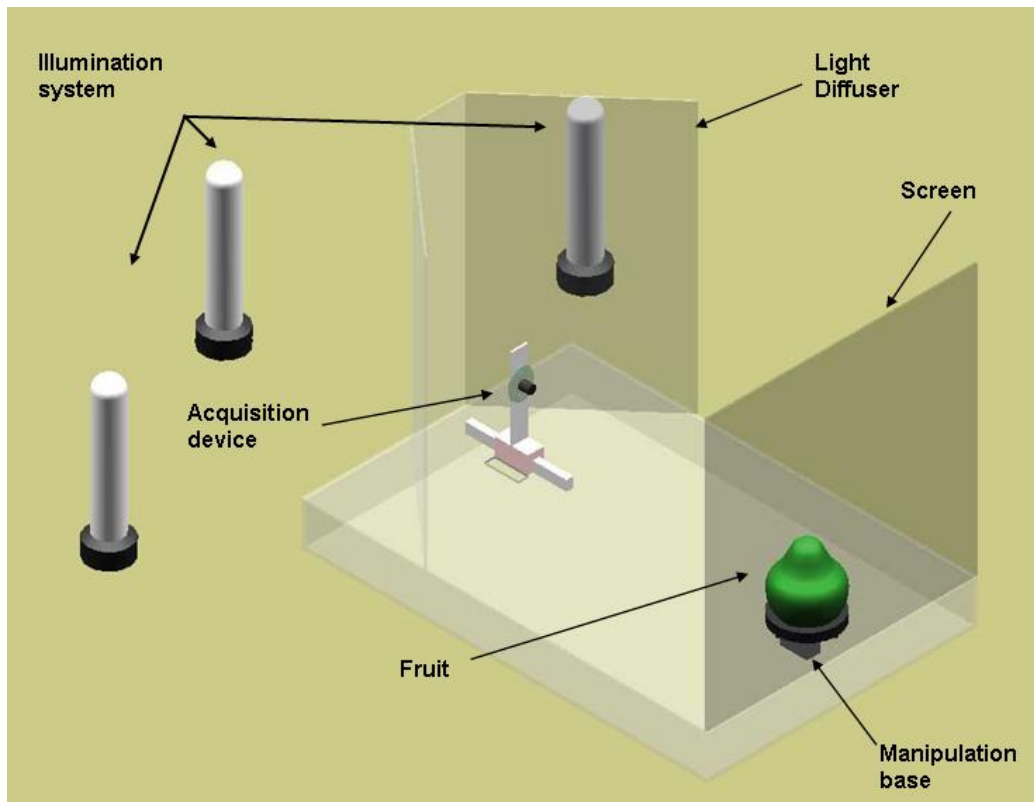


Figure 2.2: Assembled optic inspection system.

webcam and later sends a *rotate* signal to the microcontroller, via RS-232, to rotate 90 degrees the fruit and acquire the image of the other side of the fruit.

Further improvement must be done on the assembled system if a commercial prototype for fruit sorting is to be implemented. As previously mentioned (Research Aims–Page 2) our aim in this work was not to built a commercial standard prototype, instead our aim was to investigate the possibility of determining an adequate machine vision model based on physiological parameters for the appropriate sorting of guava fruit.

Image acquisition procedure

A brief description of the image acquisition procedure is mentioned involving some digital image preprocessing, whereas the rest of the image processing

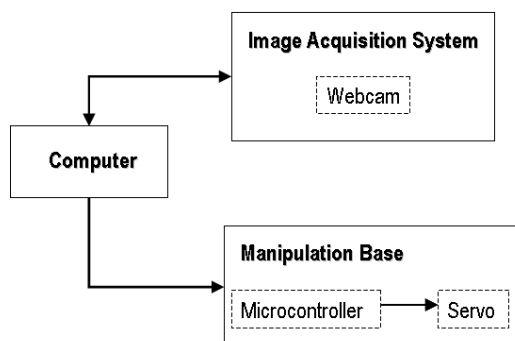


Figure 2.3: Block diagram of the assembled system.

programs will be discussed in a later section.

Corresponding to the hardware configuration, the setup is just as described in the previous section. The illumination and the light diffusers were set manually, while previewing the video input so as to obtain a good-quality image. The webcam was set using the constructed support in such fashion so that the fruit was placed in its focal plane and that the fruit occupied the most image area as possible.

A matlab script program called *capture* was developed to perform the image acquisition procedure using tools from the *image acquisition toolbox*. The program creates a videoinput object with the adaptor name `winvideo` and video format `RGB24_640x480`. Once created the videoinput object, the video resolution and other video properties are customized to perform the video preview in real time. A *manual* trigger was set and a 45 frame capturing process was enabled, so as to perform the image enhancement procedure of stacking images (section 1.5.5) to remove the electronic noise that characterized the imaging device.

A graphical user interface (GUI) was designed in order to perform the image acquisition. An image of the GUI while capturing an image is shown in Figure 2.4. By pressing the capture button the image capturing procedure is enabled while stacking images, averaging and storing them in the hard drive in “TIFF” format. This format was chosen because it is the format of choice for archiving important images. TIFF is the leading commercial and professional image standard¹.

¹Wayne Fulton. *TIFF - Tag Image File Format*, 2007. Online resource: <http://www.scantips.com/basics9t.html>

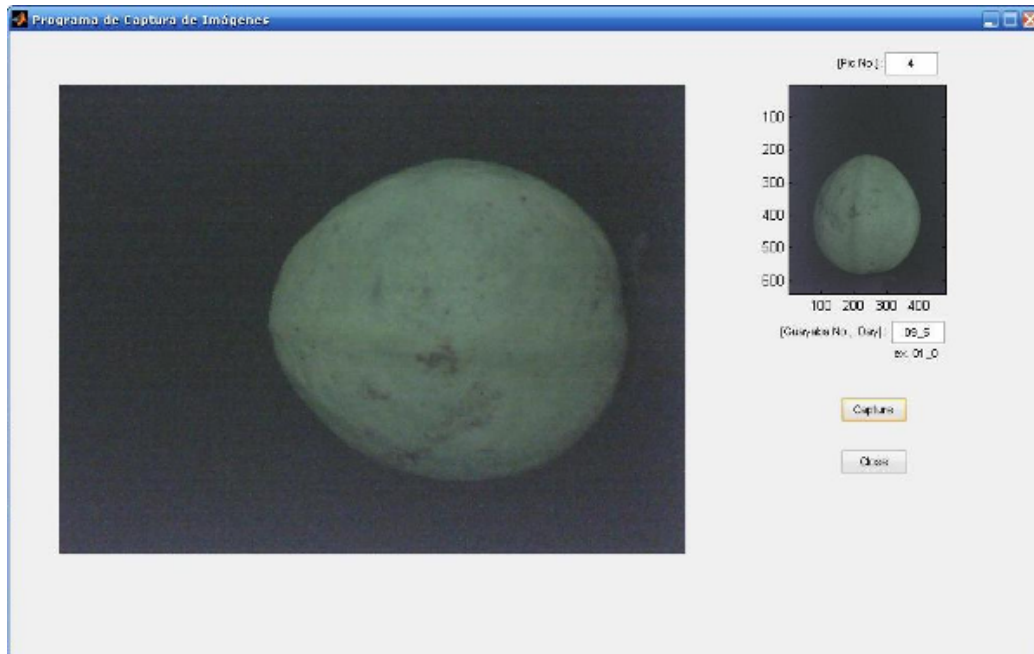


Figure 2.4: Capture GUI program.

A *rotation* signal is sent to the microcontroller a 90 degree rotation takes place and the acquisition process begins once again until the 4 images of the fruit's sides are taken.

2.3 Image processing algorithm

2.3.1 Image segmentation

Segmentation of fruit image is crucial to correct sorting, and is the foundation of feature extraction. In order to provide a correct segmentation, YCbCr color space based image segmentation algorithm was performed. At first, we convert the image from RGB color space to YCbCr color space, with the Y color feature, traditional threshold-based segmentation algorithm is utilized to segment guava area from color image; then with the priori knowledge of image, blob algorithm is used to remove noises in image.

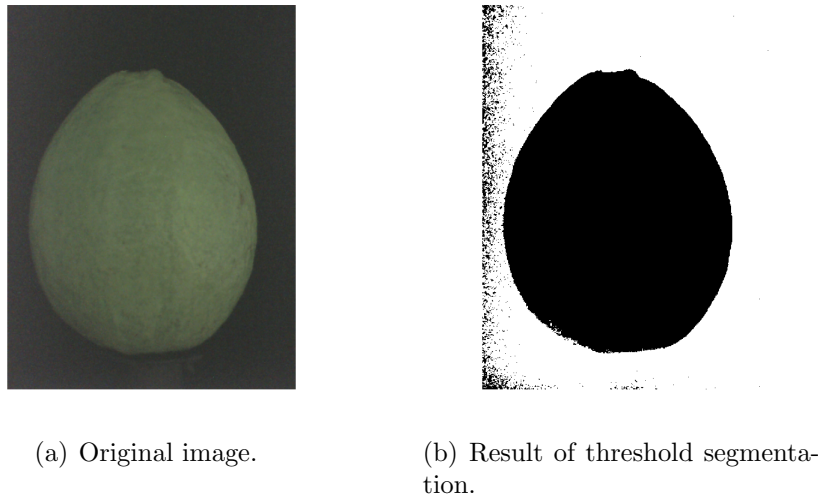


Figure 2.5: Result of image segmentation.

Conversion from RGB to YCbCr color space

A total of 8 color spaces were tested to devise which color space performed better for an adequate image segmentation. Out of the 8 spaces, the Y component of the YCbCr color space showed better performance. The conversion from RGB to the YCbCr was performed using the incorporated matlab function `rgb2ycbcr`. The function converts the truecolor image RGB to the equivalent image in the YCbCr color space YCbCr, where Y stands for luminance and Cb, Cr the chrominance color components².

Once the conversion is performed the gray-scale image is segmented via threshold-based segmentation. The same threshold was used for all of the images. The segmentation results are shown in Figure 2.5.

Blob algorithm based noise removal

Blob analysis is very important in image processing, which is used to find some blocks satisfying certain conditions in image. As the difference between the area of the guava fruit and area of image noise is quite large. we can remove noises according to the area of blob. The procedure of noises removal

²For more information on RGB to YCbCr conversion, see: Keith Jack, *YCbCr to RGB Considerations*, Intersil application note, 1997. Online resource: <http://www.intersil.com/data/an/an9717.pdf>

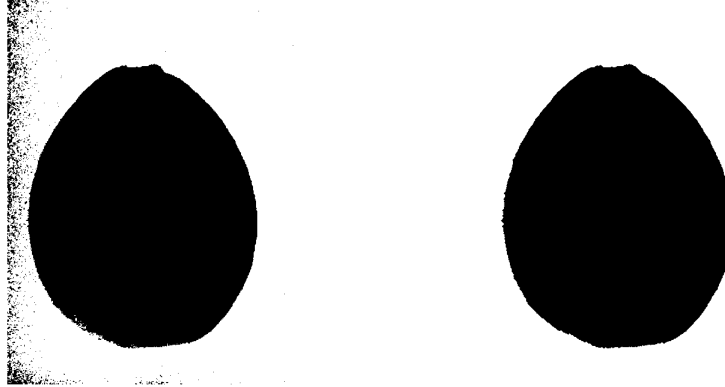


Figure 2.6: Result of blob algorithm.

is introduced below: at first, an area threshold is stated, then the blobs whose area are smaller than certain threshold will be removed from image. Since the fruit image might have some dark spots (holes) result from the threshold segmentation procedure, the image is dilated and eroded with a diamond type structuring element for further smoothing of the image. The result of blob algorithm is shown in Figure 2.6.

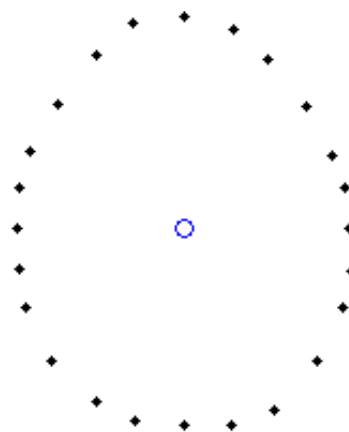
2.3.2 Spline-Interpolation based contour detection

A successful contour detection is crucial to the correct fruit shape feature extraction. From the result of image segmentation, we can see the contour of guava fruit blob is not smooth, and traditional edge detector will lose its effect in such condition, so an interpolation-based contour detection method was applied. At first, we calculate the coordinates of guava blob's geometrical center, which is adopted as original point of polar coordinate system; then we search 24 points on the contour 15 degree each; at last, spline interpolation algorithm is used to produce smooth contour of guava.

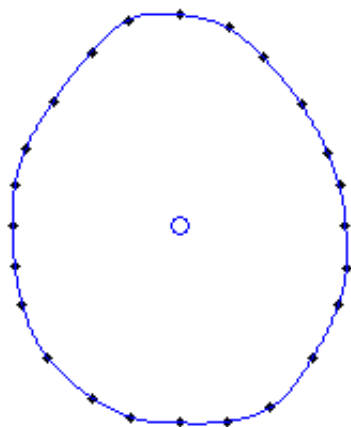
The contour detection result is shown in Figure 2.7. We can see the contour is precise and smooth enough for guavas quality feature extraction.



(a) Original image.



(b) Contour points.



(c) Spline interpolation contour.



(d) Segmented image.

Figure 2.7: Process and result of interpolation based contour detection.

2.3.3 Color feature extraction

Since the aim of the project was to study the guava fruit color behavior, once the image has been successfully segmented a color analysis was performed. The segmented image was converted from the RGB to the CIE LCH color space. The CIE LCH color space might provide a wider perception of the color change of guava. This is due to the fact that one could simply analyze the H component, also called Hue, because it is an independent color measure from the lightness or chroma (section 1.5.4). As can be seen from Figure 1.21 a change from pure green to pure yellow is equivalent to a 180-to-90 degree change. Having this in consideration we introduce the concept of *predominant color content* (PCC) in guava fruit, expressed as the highest color value (in Hue degrees) in the Hue component histogram. An important factor which was taking in account was that, since the image was segmented the background pixels are indeed the highest value in the histogram, so in fact the PCC is the second highest value in the Hue component histogram.

2.4 Guava fruit testing

The fruit testing experimental routine involved the non-destructive image acquisition procedure, the digital image analysis and the destructive experimental physical-chemical properties determination. As stated before (Research Aims–Page 2) the aim of the current work was to describe the relationships within some internal guava fruit properties and any external property determined by means of digital image analysis; Additionally if some appropriate relationships are found, develop a machine vision model that could assess in guava fruit quality sorting. The current section describes the followed methodology in this work.

Seventy (70) green fruit of the cultivar of *Psidium guajava* Cv. “Polo Nuevo” were harvested at a selected orchard near Pendales, Atlántico, Colombia. The fruits were transported under ambient conditions (2h 28°C) to the laboratory in Cartagena and stored at 25°C overnight. The next day, 7 groups of 10 fruits were randomly chosen and stored in plastic bags and held at ambient conditions for the rest of the study. During a period of 5 days each group was examined for color content, with the assembled optic system (Figure 2.2), for total soluble solids, with an Atago refractometer (model PR 201) results expressed in °Brix, and for titratable acidity by standard proce-

dures results expressed as percentage of citric acid. Two control groups were selected for daily measurements of color content only.

Out of the 50 fruits that were trialled daily, titratable acidity was not determined for 5 fruits corresponding to the first day due to difficulties in the experimental setup. So these 5 fruits were only included in the TSS evolution graph (Figure 3.1). The remaining 45 fruits were fully inspected by non-destructive and destructive means.

2.5 The similarity approach

A new assumption on the non-destructive testing procedure was evaluated. The premise is that if two guava fruit images are very similar, their internal properties, might be similar as well. It is evident that no absolute measurement related to the internal properties, was made; instead a comparison scheme was undertaken.

In section 1.5.6 the histogram refinement method was explained, which consists of splitting the pixels in a given bucket in a histogram into 2 classes, based on the coherence of the pixels. The result is called a color coherence vector (CCV). The CCV endows information not only related to the amount of pixels per bucket but information related to the distribution of these pixels.

Normalized CCVs were calculated for the 45-image dataset, corresponding to guava fruits in different maturity stages. A similarity matrix³ was built via the L_1 -distance comparison. The similarity matrix is symmetric, that is, the symmetric elements about the main diagonal are equal. For that reason only the upper triangular matrix was searched for pairs with a L_1 -distance value in the range $(0 < x < 0.2)$. This was the criteria used for considering 2 guava fruit images to be similar to one another. A detailed description of the process is observed on Figure 2.8.

³For a further discussion on these concepts: see Appendix B

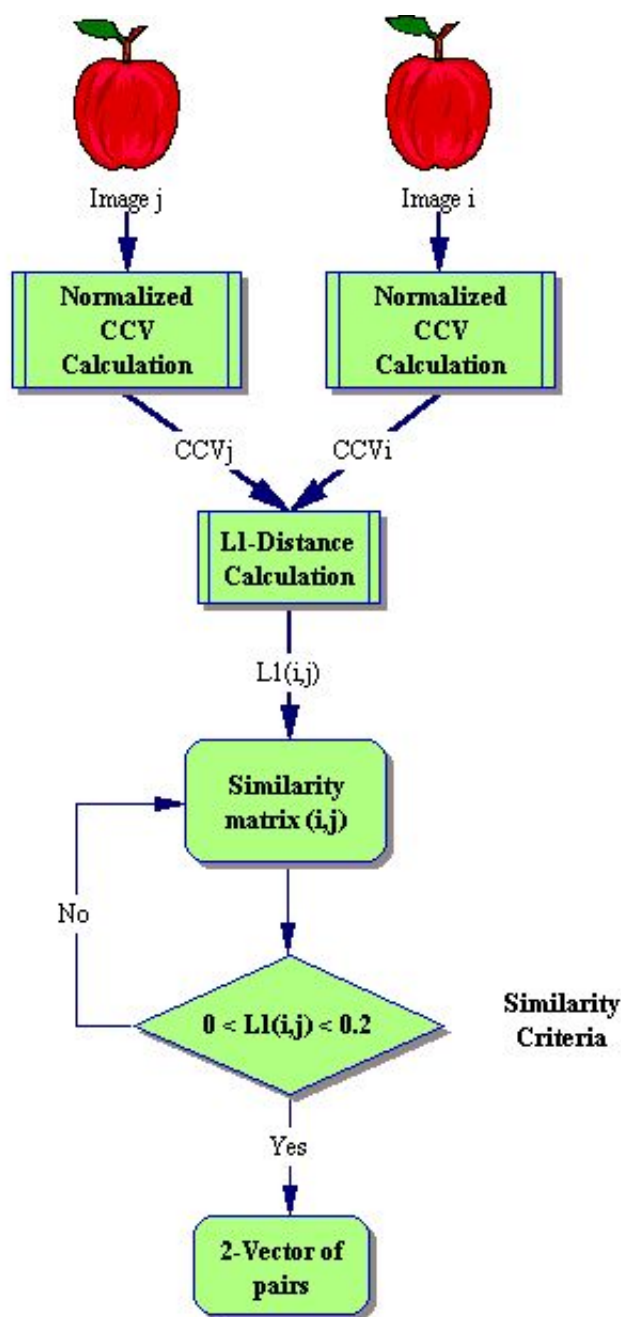


Figure 2.8: Similarity procedure. Image comparison using the L1-distance on normalized CCVs.

Chapter 3

Results

The results for the different tests performed on the study-set are shown in the following subsections. A statistical analysis is performed so as to validate the results found.

3.1 Destructive testing

As previously mentioned destructive tests (Total soluble solids and titratable acidity) were performed on the guava fruits. The results for the evolution of soluble solids, titratable acidity and the maturity index are shown in the following subsections.

3.1.1 Evolution of total soluble solids

Figure 3.1 shows a rapid increase of the total soluble solids during ripening (6.74 - 9.86 °Brix) followed by a slower decrease to 7.25 °Brix on the maturity stage with an increase on the final day to 9.29 °Brix. The decrease probably happened because of high consumption of sugars due to the respiration rate (Singh, Singh et al. [54]; Sharaf and El-Saadany [55]). Soares et al.(2007) [56] reported similar behavior for guava cultivar Cortibel. The authors showed the increase of the content of soluble solids of guava with maturation with a decrease on the maturity stage. The results obtained were: between 7.40, 8.60 and 8.4 °Brix.

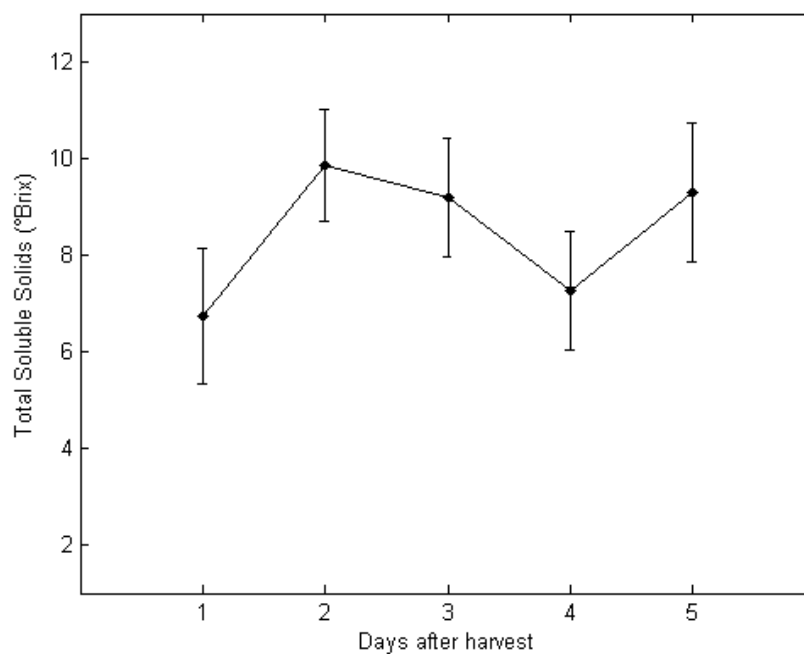


Figure 3.1: Total soluble solids content of *P. guajava* during storage at ambient conditions. Vertical bars indicate \pm SD.

3.1.2 Titratable acidity

Titratable acidity increased in the immature and intermediary stage of maturation and decreased in the maturity stage with a slight but not significant increase in the last day. Increase in the titratable acidity shows the formation of organic acids during maturation. This increase is associated with the high concentration of undissociated organic acids, stored in the vacuole and the fruits use these acids as respiratory substrate (Medlicott and Jeger [57]). Bashir, Abu-Goukh and Abu-Bakr (2003) [58] reported similar results to pink and white guava pulp. Titratable acidity increased from 0.15% to 0.19% of citric acid up to the climacteric peak and declined thereafter from 0.19% to 0.154% citric acid for white guava.

3.1.3 Maturity Index

The maturity index was calculated by equation 1.2 given by (Parra and Hernandez [22]). The maturity index (I_m) is used to describe the general

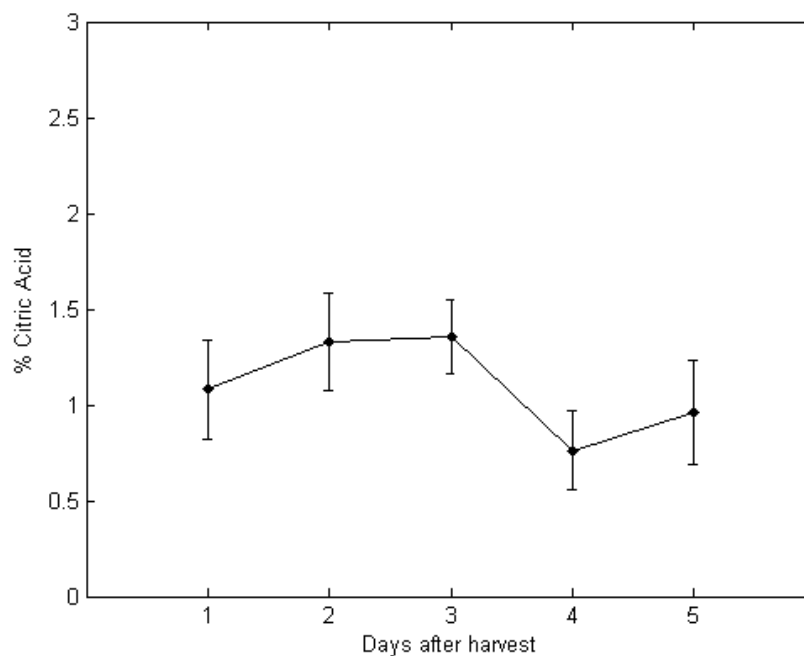


Figure 3.2: Titratable acidity of *P. guajava* during storage at ambient conditions expressed as % of citric acid. Vertical bars indicate \pm SD.

ripening evolution in post-harvest as the ratio between the total soluble solid contents and the percentage of the predominant acid in the pulp of the fruit.

The I_m overall behavior was a smooth increase from 5.31 to 8.48 as the ripening process endured with a minor decrease on the third day after harvest. This behavior is evident from the rapid initial increase in total soluble solid contents, despite the fact that the citric acid percentage slightly increases in the first stage. Figure 3.3 suggests that when the fruit has reached the maturity stage a I_m around 8 should be expected given by days 4 and 5 of the study. Jha, Chopra et al. (2007) [59] reported a predicted I_m , solely based on TSS, which could be used as means to determine the proper maturity stage supported by a sensory panel score.

3.2 Non-Destructive testing

The non-destructive testing procedure involved basically the digital image analysis by mean of the predominant color content (PCC). Typical segmented

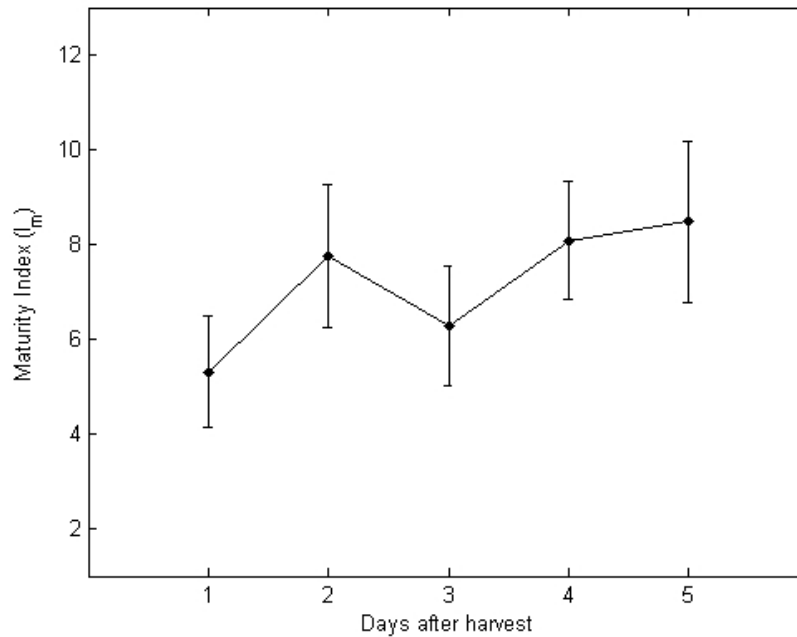


Figure 3.3: Maturity index (I_m) of *P. guajava* during storage at ambient conditions. Vertical bars indicate SD.

images for analysis are shown in Figure 3.4. The PCC evolution from 10 guavas from the control group is shown in Figure 3.5.

From Figure 3.5 an overall tendency to decrease is observed. There is difficulty in comparing the different curves since, apparently, each guava has its own path. Notice that these are individual color behaviors for each guava because these fruits were not destroyed. Their color was measured during each day of the study. For being able to truly compare these curves with one another, a normalization procedure took place. The results from the normalized curves are shown in Figure 3.6.

As expected, from Figure 3.6 a decreasing behavior can be suggested with greater confidence. The decreasing behavior comes from the change from green to yellow, which measured in Hue degrees corresponds to a change from 180-to-90 degrees. This behavior is depicted from the same figure.

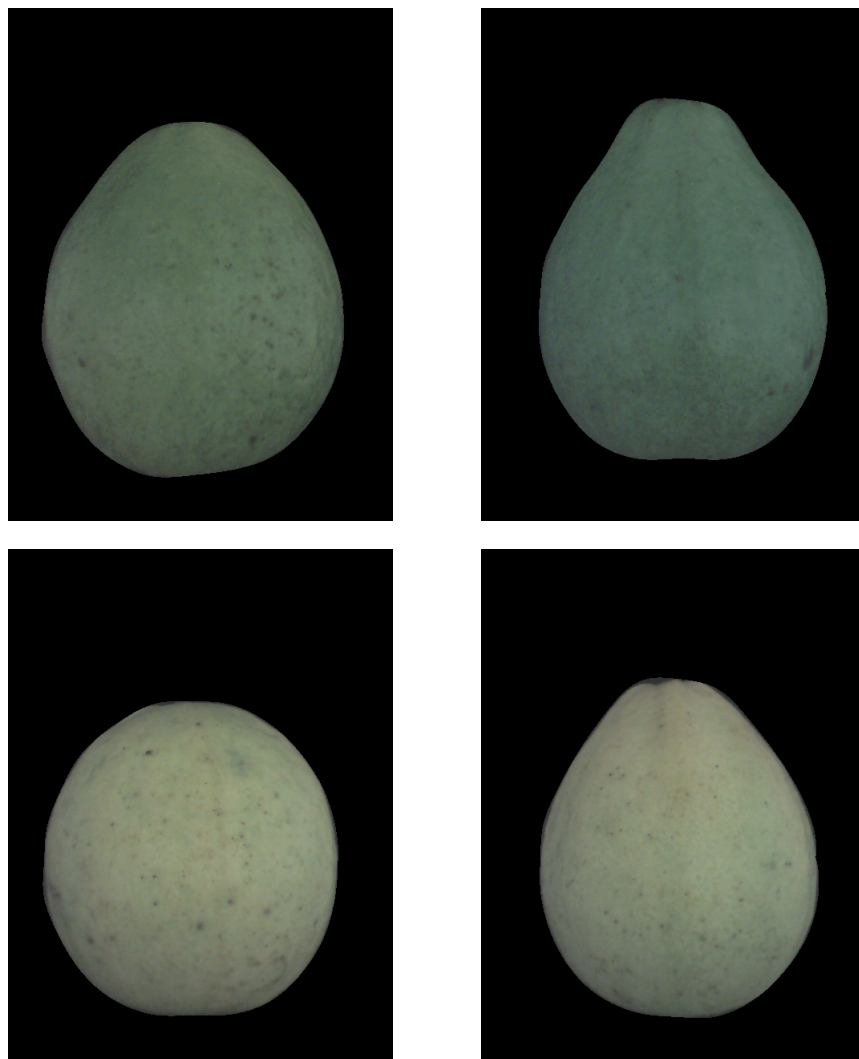


Figure 3.4: Segmented images of different guavas used for the PCC measurements.

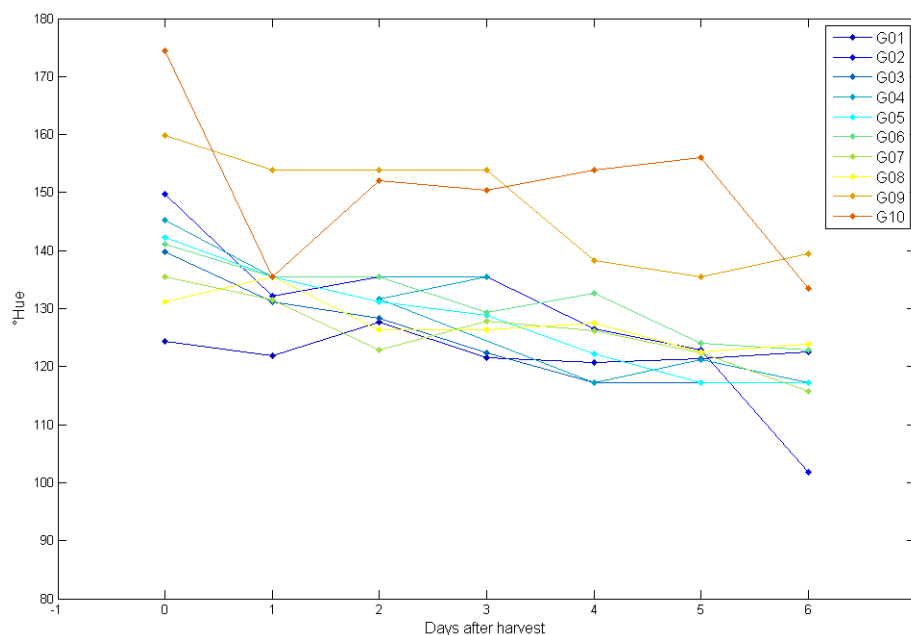


Figure 3.5: Predominant color content evolution in 10 guavas from the control group.

3.3 Data analysis

3.3.1 A first descriptive analysis

A first descriptive analysis was done so as to inspect a relationship among the measured internal properties and the external color content. In Figure 3.7 superposed curves corresponding to the maturity index and the average PCC evolution are shown. An initial difficulty arises when considering solely the PCC as a descriptor for trying to predict the internal behavior. An overall decreasing behavior was mentioned in the previous section, which is depicted from this curve. While the maturity index, as well as the soluble solids and the titratable acidity fail to behave in the same way, as they do not increase or decrease continuously, due to their metabolic behavior.

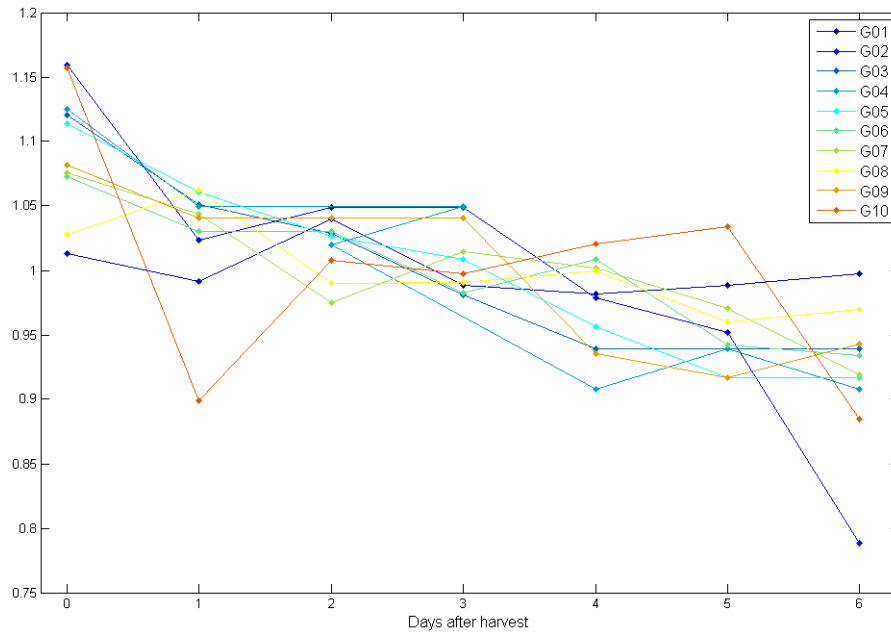


Figure 3.6: Normalized predominant color content evolution in 10 guavas from the control group.

3.3.2 Statistical analysis

CIELab and CIELCh color space transformations (Sections 1.3.1, 1.5.4) were performed on the segmented images for color analysis. Median L, a, b, c and hue values were obtained for all of the segmented images.

Our first approach was to evaluate the possibility to correlate the measured TSS, the titratable acidity and the calculated I_m with the measured color values to be able to non-destructively determine the maturity level.

Measured L, a, b, c and hue values were exported to STATGRAPHICS Centurion, a statistical software package, for multivariate analysis.

In order to search for the best relationships for predicting TSS, titratable acidity (TA) and I_m from L, a, b, c and hue values, regression model selection procedure (RMSP)¹ was performed on the data. The RMSP helps in the selection of independent variables used in a multiple regression model to predict a single quantitative dependent variable. The procedure considers all possible regressions involving different combinations of the independent

¹For a further discussion on these concepts: see Appendix A

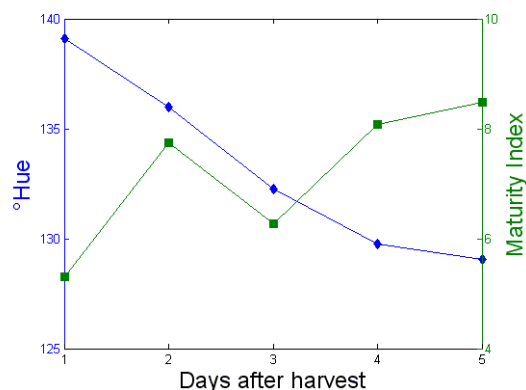


Figure 3.7: Maturity index and average PCC evolution.

variables.

Various multiple regression models (MRM) were fit to describe the relationship between TSS, TA and I_m , and 12 predictor variables. The predictor variables are based on the measured color values and some arithmetic transformation of the same. Models were fit containing all combinations of from 1 to 8 variables. The best model for each case (table 3.1), the statistics tabulated (table 3.2) and the resulting adjusted R-squared plot are as follows.

Model No.	Variables	Models*
1	$L, L^2, h^2, a \times b$	$TSS = C_1 + C_2L + C_3L^2 + C_4h^2 + C_5ab$
2	$c, c^2, h^2, c \times h$	$TA = C_1 + C_2c + C_3c^2 + C_4h^2 + C_5ch$
3	c, L^2	$I_m = C_1 + C_2c + C_3L^2$

* C_1, C_2, C_3, C_4, C_5 are models constants.

Table 3.1: Generalized forms of the best TSS, TA and I_m fit models in terms of color values (L, a, b, c, h)

The adjusted R^2 statistic measures the proportion of the variability in TSS, TA and I_m that are explained by their corresponding model. From a model that significantly represents a given property, large values of the adjusted R^2 and small values of MSE are to be expected. None of the determined models accomplish such criteria. Out of the three models, model no. 1 is the one with the largest adjusted R^2 and yet it explains roughly a 31.5 percent of the variability of TSS.

Adjusted R^2 plots for TSS, TA and I_m are shown in Figure 3.8. The plots

Model No.	MSE	R ²	Adjusted R ²	Cp
1	2.85525	37.7432	31.5175	-0.53255
2	0.23158	24.1810	16.5991	-0.42421
3	7.68124	26.8527	23.3695	-4.00097

Table 3.2: Statistical results of the best models for determining TSS, TA and I_m .

show that not necessarily incrementing the number of descriptor variables improves the model's performance. For the first two cases the best model is obtained with 5 descriptor variables and for the third case roughly 2 variables achieve the best performance.

These results allow us to formulate a certain hypothesis regarding the relationship of the TSS and TA towards the predominant color content. It appears that the internal properties, specifically TSS and TA, do not completely determine guava fruit external color content and that more non-destructive information must be acquired (i.e. respiration rate, CO₂ production) in order to obtain a more accurate model that describes the ripening behavior. This hypothesis can be partially sustained with the previous results and by analyzing the measured properties using a multifactor ANOVA test.

The multifactor ANOVA procedure is designed to construct a statistical model describing the impact of two or more factors on a dependent variable. Tests are run to determine whether or not there are significant differences between the means of the dependent variable and the different levels of the factors and whether or not there are interactions between the factors.

In order to perform the multifactor ANOVA test the measured TSS and TAs were categorized on 5 different levels with equally spaced ranges (table 3.3). The multifactor ANOVA test was carried out considering the predominant color value, expressed in hue, as the dependent variable and the TSS and TA as the independent variables. This was done this way so that we could establish if there are considerable effects of the TSS and TAs on the predominant color content.

A scatter plot for the different TSS and TA levels is shown in Figure 3.9. Both plots suggest that there are no differences between the different levels of TSS and TA; that is, samples with high and low TSS and TA values possess the same predominant color content.

With the purpose of determining whether or not the TSS and TA values have a significant effect on the predominant color content, an analysis of

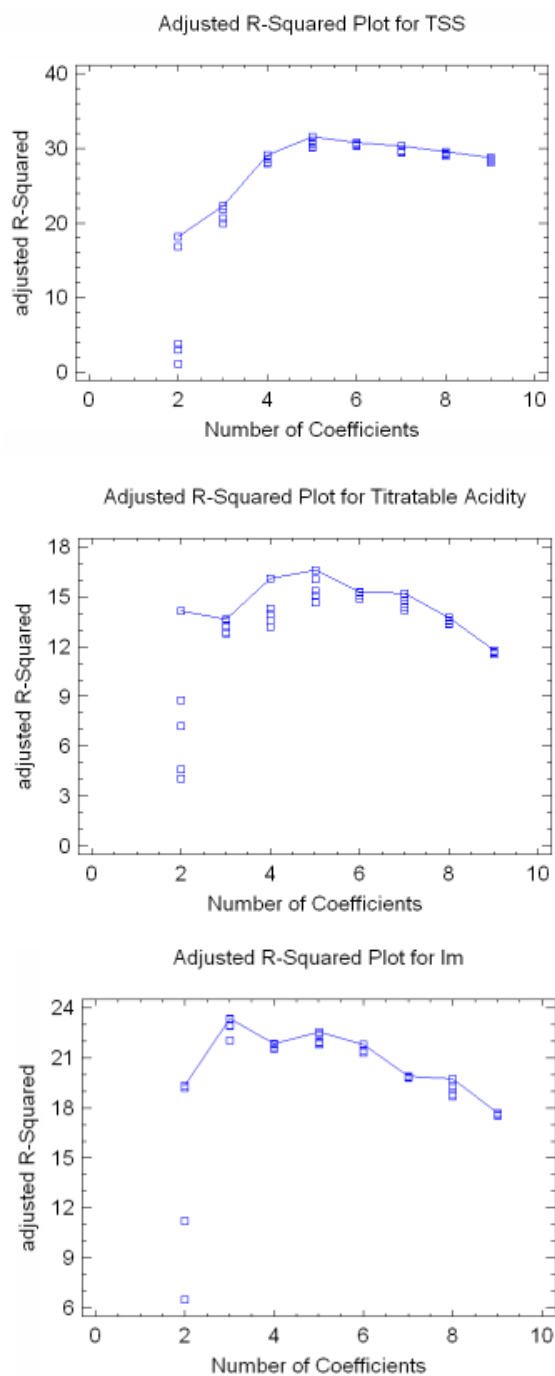


Figure 3.8: Adjusted R^2 plots for TSS, TA and I_m .

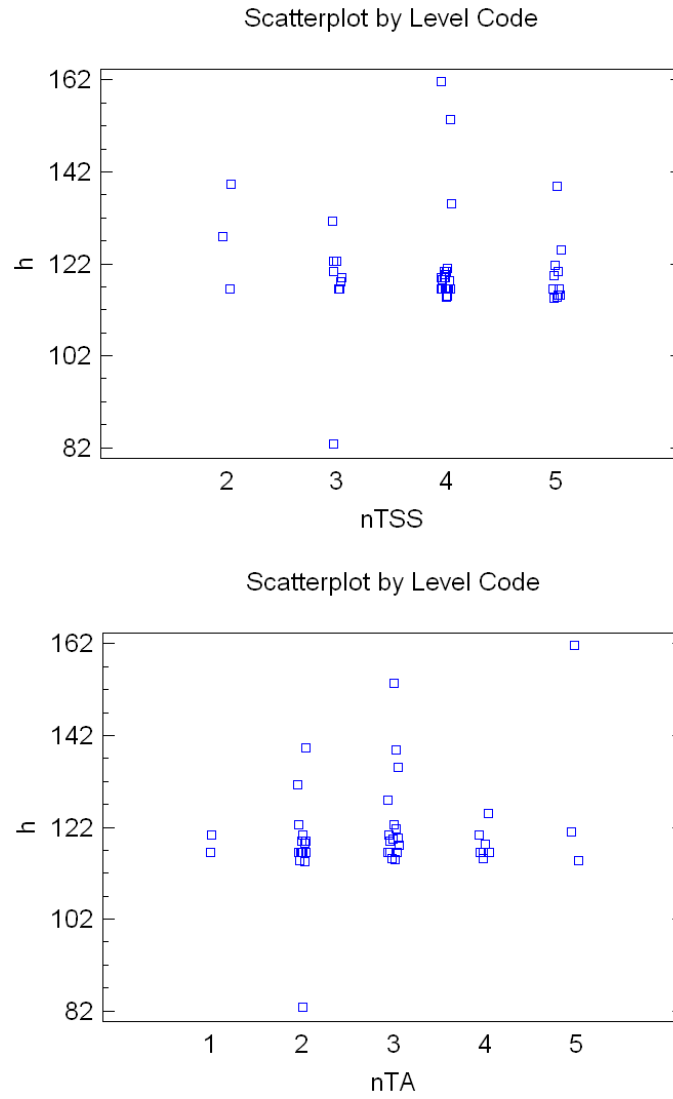


Figure 3.9: TSS and TA scatterplot by level Code.

Level	TSS range (°Brix)*	TA range (% of citric acid)*
1	0.0 – 2.4	0.00 – 0.54
2	2.4 – 4.8	0.54 – 1.08
3	4.8 – 7.2	1.08 – 1.62
4	7.2 – 9.6	1.62 – 2.17
5	9.6 – 12.0	2.17 – 2.71

* all intervals are half-closed by the right-hand term (*i.e.* $0 < x \leq 2.4$).

Table 3.3: TSS and TA levels.

variance is performed. The results are displayed in table 3.4.

Source	Sum of Squares	Df	Mean Square	F-Ratio	P-Value
MAIN EFFECTS					
A:nTSS	284.657	3	94.8856	0.75	0.5300
B:nTA	621.327	4	155.332	1.23	0.3166
RESIDUAL	4688.5	37	126.716		
TOTAL (CORRECTED)	5695.91	44			

All F-ratios are based on the residual mean square error.

Table 3.4: Analysis of Variance for h - Type III Sums of Squares. “h” stands for PCC measured in hue degrees.

The ANOVA table decomposes the variability of h^2 into contributions due to various factors. Since Type III sums of squares have been chosen, the contribution of each factor is measured having removed the effects of all other factors. The P-values test the statistical significance of each of the factors. Since no P-values are less than 0.05, none of the factors have a statistically significant effect on h at the 95.0% confidence level.

In view of the fact that no direct relationships could be found between TSS and TAs with the predominant color content a different approach towards non-destructive guava fruit testing must be pursued. The results for the similarity approach are presented in the present section.

A similarity matrix was built via the L_1 -distance comparison³. Out of the 990 elements of the upper triangular matrix (discarding the main diagonal)

²“h” stands for PCC measured in hue degrees.

³For details on these calculations see Section 2.5

89 pairs were found to be in correspondence with the similarity criteria. The result was stored in a 2-column similarity vector. The corresponding TSS, TA and I_m values for each guava fruit were mapped to the obtained similarity vector.

With the intention of establishing if the paired guava fruits, by the similarity criteria, possess similar internal properties a statistical two-sample comparison (t-test) was carried out. The goal is to determine if there are significant differences between the means, variances, and/or medians of the samples. It is assumed that no relationship exists between a selected observation in one sample and any specific observation in the other sample. Three 2-column vectors of 89 elements, each vector corresponding to the mapped TSS, TA and I_m values, were analyzed with the t-test.

To be able to run a t-test over the samples it is necessary to establish that the samples come from normal distributions. A normality test was performed on the data (table 5) using the standardized kurtosis test which looks for distributional shape which is either flatter or more peaked than the normal distribution.

Data set	Statistic	P-value
TSS1 - TSS2	1.00551	0.314651
TA1 - TA2	0.072835	0.941931
I_{m1} - I_{m2}	0.807395	0.419437

Table 3.5: Tests for Normality using the Kurtosis Z-score test.

Since all of the P-values from the tests performed are greater than or equal to 0.05, we can not reject the idea that all samples come from a normal distribution with 95% confidence. A summary statistics table for the dataset is shown in table 3.6.

From the summary statistics (table 3.6) is apparent that the 3 paired datasets possess similar measures of central tendency and dispersion with minor differences between the I_{m1} and I_{m2} samples.

Results for the t-test for comparison of the means of the paired datasets as well as the determined confidence bounds for each mean and the difference between the means are shown in tables 3.7–3.9. Of particular interest are the confidence intervals for the difference between the means of TSS1-TSS2, TA1-TA2 and I_{m1} - I_{m2} , which extend from -0.160216 to 0.908531, from -0.247064 to 0.0607719 and from -0.568722 to 1.39839, respectively. Since all

	TSS1	TSS2	TA1	TA2	Im1	Im2
Count	89	89	89	89	89	89
Average	8.72135	8.34719	1.24056	1.33371	7.9364	7.52157
Standard deviation	1.66961	1.93327	0.459761	0.574429	2.96668	3.64747
Coeff. of variation (%)	19.144	23.1607	37.0607	43.0701	37.3807	48.4934
Minimum	4.0	4.0	0.48	0.48	2.22	2.22
Maximum	12.0	11.5	2.71	2.71	14.93	16.51
Range	8.0	7.5	2.23	2.23	12.71	14.29

Table 3.6: Summary statistics.

95.0% confidence interval for mean of TSS1:	8.72135 +/- 0.351708	[8.36964, 9.07306]
95.0% confidence interval for mean of TSS2:	8.34719 +/- 0.407248	[7.93994, 8.75444]
95.0% confidence interval for the difference between the means assuming equal variances:	0.374157 +/- 0.534374	[-0.160216, 0.908531]
t-test to compare means		
Null hypothesis:	mean1 = mean2	
Alt. hypothesis:	mean1 NE mean2	
Assuming equal variances:	t = 1.38183	P-value = 0.168775

Table 3.7: Comparison of means TSS1 - TSS2.

95.0% confidence interval for mean of TA1:	1.24056 +/- 0.0968499	[1.14371, 1.33741]
95.0% confidence interval for mean of TA2:	1.33371 +/- 0.121005	[1.2127, 1.45471]
95.0% confidence interval for the difference between the means assuming equal variances:	-0.0931461 +/- 0.153918	[-0.247064, 0.0607719]
t-test to compare means		
Null hypothesis:	mean1 = mean2	
Alt. hypothesis:	mean1 NE mean2	
Assuming equal variances:	t = -1.19432	P-value = 0.23396

Table 3.8: Comparison of means TA1 TA2.

95.0% confidence interval for mean of Im1:	7.9364 +/- 0.62494	[7.31146, 8.56134]
95.0% confidence interval for mean of Im2:	7.52157 +/- 0.768349	[6.75322, 8.28992]
95.0% confidence interval for the difference between the means assuming equal variances:	0.414831 +/- 0.983554	[-0.568722, 1.39839]
t-test to compare means		
Null hypothesis:	mean1 = mean2	
Alt. hypothesis:	mean1 NE mean2	
Assuming equal variances:	t = 0.832375	P-value = 0.406325

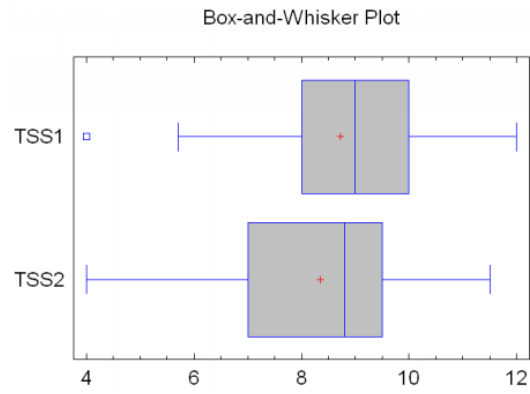
Table 3.9: Comparison of means Im1 - Im2.

intervals contain the value 0, there is not a statistically significant difference between the means of each of the paired datasets at the 95.0% confidence level.

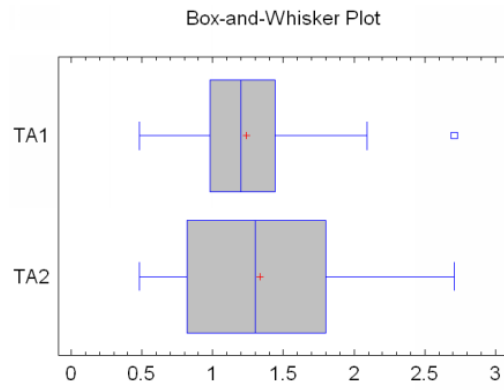
The t-test was constructed to determine whether the difference between the two means equals 0.0 versus the alternative hypothesis that the difference does not equal 0.0. Since the computed P-value for all of the tests (tables 3.7–3.9) are not less than 0.05, we cannot reject the null hypothesis.

The box and whiskers plots are shown in Figure 3.10. Each of the central tendency measures appear to be in the same range, as previously determined, except for some skewness present in the Im1-Im2 plot (Figure 3.10(c)). Only for the TA1-TA2 plot (Figure 3.10(b)) is TA2 box considerably wider than the TA1 box, which corresponds to greater variability. In all plots there is at least one outside point that could be regarded as an outlier. Since all box plots overlap significantly there is indication that a noticeable relations exists among the compared data.

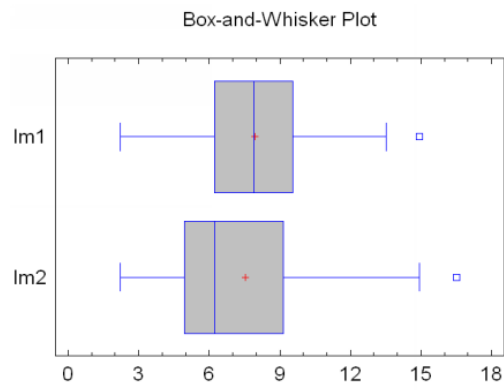
In order to determine by other graphical means the comparison of the distribution of the paired datasets, quantile-quantile plots (Figure 3.11) were used. Of special interest is the evident tendency towards linearity near the center, especially in the TSS and I_m plots, which highly suggests that the null hypothesis, based on a 1-to-1 relationship, cannot be rejected. In other words, if the two samples came from the same underlying population the points should lie approximately along the diagonal line. This allows us to consider a high internal similarity between the predicted, by an external similarity approach, paired samples.



(a)

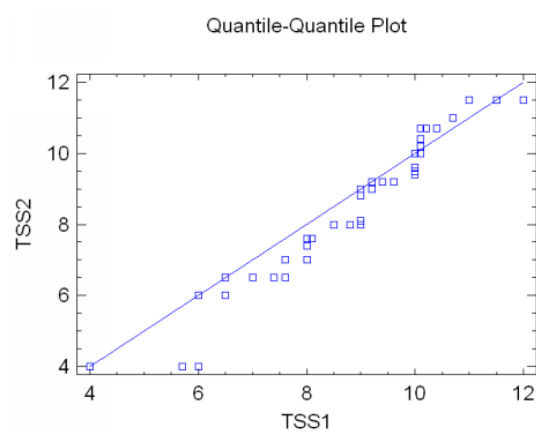


(b)

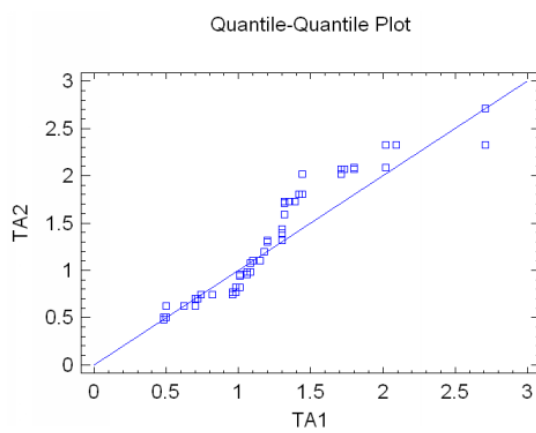


(c)

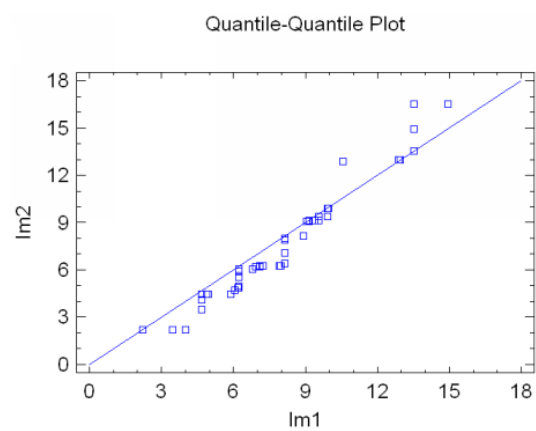
Figure 3.10: Box and whisker plots.



(a)



(b)



(c)

Figure 3.11: Quantile-Quantile plots.

3.4 Discussion

The current study enclosed destructive and non-destructive testing of *Psidium guajava* for ripeness determination. The main objective was to establish by non-destructive means, specifically by digital image analysis measuring the predominant color content in fruit, the fruits internal ripeness degree. In order to achieve such objective, traditional physical-chemical internal parameters (Titratable acidity and Total soluble solids) were measured and a maturity index was calculated.

The observed behavior for TSS and TA was expected as reported in literature. It is clear that regardless of the decrease of TSS contents, probably due to consumption of sugars driven by the respiration rate, the I_m reflects the nature of the ripening process since it beholds the decrease in titratable acidity in the maturity stage.

Color measurements made from the guava fruits did not encompass a reliable relation with the measured internal properties demonstrated with a multifactor ANOVA test. Consequently no model with a sustaining prediction was found. It appears that the internal properties, specifically TSS and TA, do not completely determine guava fruit external color content and that more non-destructive information must be acquired (i.e. respiration rate, CO₂ production) in order to obtain a more accurate non-destructive model that describes the ripening behavior. Further research is needed. To our knowledge, in literature there is only one work (Jha, Chopra et al. 2007 [59]) which establishes a model for predicting maturity index using color values of mango. Although apparent good performance is achieved, color values are measured with a handheld colorimeter at selected points in the fruit, no global description of the fruit is obtained so as to implement a capable sorting system.

The similarity approach shows promise. The argument that two similar guava fruit images represent similar internal properties shows recognizable correlation (Figure 3.11). The advantage of this approach is that more information is employed. Not only all color content of the fruit is examined but its distribution as well. More research is needed so as to determine a plausible conclusion.

Chapter 4

Conclusions

There are many possible methods for non-destructive testing of guava fruit. We have shown here that Optic inspection by means of digital image analysis shows promise to be capable of testing guava fruit ripeness and have designed a system that could be capable of doing such task. The overall color measurements made from the studied guava fruits did not exhibit a solid relation with the measured internal properties (TSS and TA), probably due to respiration rate patterns and the fact that apparently TSS and TA do not completely determine the fruit external color. The similarity approach showed recognizable success in carrying out a comparison scheme for predicting guava fruit ripeness degree. More investigation is needed.

4.1 Future work

There are still many possible methods for detecting guava fruit ripeness, beyond the improvement of the proposed system and validating the similarity method, other possible research includes the use of other sensors and the development of an integral quality measurement algorithm where not only ripeness degree is considered, defects detection, shape and other properties that would allow the development of adequate sorting criteria.

Appendix A

Statistical analysis

A.1 Regression model selection

The **Regression Model Selection** procedure is designed to help select the independent variables to use in building a multiple regression model to predict a single quantitative dependent variable Y . The procedure considers all possible regressions involving different combinations of the independent variables. It compares models based on the adjusted R-Squared, Mallows Cp statistic, and the mean squared error.

Models are fit involving all combinations of variables. The results are shown in a table with the following elements.

A.1.1 MSE

The mean squared error. This is an estimate of the variance of the deviations from the fitted model, given by:

$$MSE = \frac{\sum_{i=1}^n (y_i - \hat{y}_i)^2}{n - p - 1}$$

where y_i is the observed value of Y , \hat{y}_i is the predicted value from the fitted model, and p equals the number of independent variables included in the model.

A.1.2 R-Squared

The adjusted coefficient of determination, calculated from:

$$R^2 = 100 \left(1 - \frac{\sum_{i=1}^n (y_i - \hat{y}_i)^2}{\sum_{i=1}^n (y_i - \bar{y}_i)^2} \right)$$

R-Squared measures the percentage of the variability in Y that has been explained by the fitted model.

A.1.3 Adjusted R-Squared

The adjusted coefficient of determination, calculated from:

$$R_{adj}^2 = 100 \left(1 - \left(\frac{n-1}{n-p-1} \right) \frac{\sum_{i=1}^n (y_i - \hat{y}_i)^2}{\sum_{i=1}^n (y_i - \bar{y}_i)^2} \right)$$

The adjusted R-Squared compensates for the number of independent variables in the model. It is more useful than the ordinary R-Squared in comparing model with different numbers of independent variables, since the latter statistic will never go down even if unrelated variables are added to the model.

A.1.4 Cp

Mallow's Cp statistic, calculated from:

$$C_p = \frac{\sum_{i=1}^n (y_i - \hat{y}_i)^2}{MSE(full) - (n - 2p)}$$

where $MSE(full)$ is the mean squared error of the model when all independent variables are included in the fit. If a fitted model has little bias, C_p should be close to p . It is desirable to have a small C_p , as long as the value is not much greater than p .

A.2 Multifactor ANOVA

The **Multifactor ANOVA** procedure is designed to construct a statistical model describing the impact of two or more categorical factors X_j on a dependent variable Y . Tests are run to determine whether or not there are significant differences between the means of Y at the different levels of the factors and whether or not there are interactions between the factors. In addition, the data may be displayed graphically in various ways, including a multiple scatterplot, a means plot, and an interaction plot.

In order to determine whether or not the factors have a significant effect on the dependent variable, the analysis of variance is performed. Results are displayed in a typical ANOVA Table:

Source	Sum of Squares	Df	Mean Square	F-Ratio	P-Value
MAIN EFFECTS					
A:body fat	702.25	1	702.25	79.10	0.0000
B:gender	210.25	1	210.25	23.68	0.0000
C:smoking	343.056	2	171.528	19.32	0.0000
INTERACTIONS					
AB	2.25	1	2.25	0.25	0.6189
AC	204.167	2	102.083	11.50	0.0003
BC	21.5	2	10.75	1.21	0.3142
RESIDUAL	230.833	26	8.87821		
TOTAL (CORRECTED)	1714.31	35			

All F-ratios are based on the residual mean square error.

Table A.1: An example of an analysis of variance for “minutes” - Type III Sums of Squares.

The table divides the overall variability among the n measurements into several components:

1. A component attributable to the *Main Effect* of each factor, which measures the variability amongst the mean responses at each level of the factor.
2. A component attributable to the *Interaction* between different factors. An interaction occurs if the effect of one factor depends on the level of another factor.

3. If *Covariates* are present, a component attributable to each covariate.
4. A *Residual* component, which measures the variability amongst subjects at identical levels of the factors

Of particular importance are F-ratios and their associated P-Values. Small P-Values (less than 0.05 if operating at the 5% significance level) correspond to significant effects.

In the current example, all of the main effects are statistically significant as is the interaction between factors A and C (*Body fat* and *Smoking*).

Appendix B

Mathematical Tools

B.1 The L1-distance

The L₁-distance is a metric in which the distance between two points is the sum of the absolute differences of their coordinates. In this work we refer to the L₁-distance as means to establish a score for a comparison between the normalized *color coherence vectors* (CCV) of two different images. The L₁-distance between two given CCVs is expressed as:

$$\Delta_{CCV} = \sum_{j=0}^N \left| (\alpha_j - \alpha'_j) \right| + \left| (\beta_j - \beta'_j) \right|$$

It is mandatory to normalize the CCVs to be able to apply the L₁-distance. Knowing that the CCVs are normalized, the trivial L₁-distance scores would be “0” and “2”, corresponding to a comparison between the same image or two completely different images, respectively.

B.2 The similarity matrix

A similarity matrix is a matrix of scores which express the similarity between two data points. In this work the similarity matrix is used as means to compare two datasets of images, where the score is based on the L₁-distance. An example of what a similarity matrix would look like:

	a	b	c
a	0	0.1	1.2
b	0.1	0	0.5
c	1.2	0.5	0

In this example, the main diagonal represents the trivial case of comparing an image with itself. From the same matrix, a and b are very similar due to a low score of 0.1.

Bibliography

- [1] A. Mizrach, U. Flitsanov, Z. Schmilovitch, and Y. Fuchs. Determination of mango physiological indices by mechanical wave analysis. *Postharvest Biology and Technology*, 16:179–186, 1999.
- [2] Robert K. McConnell and Henry H. Blau. Color classification of non-uniform baked and roasted foods. Online resource: <http://www.way2c.com/w2bkrst.php>, 1996.
- [3] Rafael Gonzalez and Richard Woods. *Digital Image Processing*. Prentice Hall, Upper Saddle River, 2nd edition, 2002.
- [4] Guo Feng and Cao Qixin. Study on color image processing based intelligent fruit sorting system. In *Proceedings of the 5th World Congress on Intelligent Control and Automation*, pages 4802–4805, Hangzhou, P.R. China, June 2004.
- [5] F. Pla, J.M. Sanchiz, and J.S. Sánchez. An integral automation of industrial fruit and vegetable sorting by machine vision. *8th IEEE International Conference on Emerging Technologies and Factory Automation*, 2:541 – 546, 2001.
- [6] Philippe Cattin. *Digital Image Fundamentals*. ETH Zurich, 2006. Computer vision laboratory.
- [7] Robert Fisher, Simon Perkins, Ashley Walker, and Erik Wolfart. Hypermedia image processing reference. Online resource: <http://homepages.inf.ed.ac.uk/rbf/HIPR2/wksheets.htm>, 2000.
- [8] Jairo Perez. Estudio de la cadena logística de los productos agrícolas que se producen en la zona norte del departamento de bolívar para identificar

- estrategias que faciliten su comercialización. Master's thesis, Universidad Autónoma de Bucaramanga - Instituto de Estudios Superiores de Monterrey - Universidad Tecnológica de Bolívar, 2004.
- [9] J.J. Báez Rojas, M.L. Guerrero, J. Conde Acevedo, A. Padilla Vivanco, and G. Urcid Serrano. Segmentación de imágenes de color. *Rev. Mex. Fís.*, 50(6):579–587, 2004.
- [10] N. Laguado, M. Marín, L. Arenas, and C. Castro. Relación entre variables indicadoras de maduración de frutos de guayabo (*psidium guajava* l.) var. dominicana roja. *Rev. Fac. Agron. (LUZ)*, 15:422–428, 1998.
- [11] Belén Diezma and Margarita Ruiz-Altisent. Propiedades acústicas aplicadas a la determinación de los parámetros de calidad interna de productos hortofrutícolas. *Revista de Acústica*, 35(1,4):20–25, 2004.
- [12] Judith A. Abbott. Quality measurement of fruits and vegetables. *Postharvest Biology and Technology*, 15:207–225, 1999.
- [13] A Mizrach, N. Galili, and C. Rosenhouse. Determination of fruit and vegetable properties by ultrasonic excitation. *Trans. ASAE*, 32:2053–2058, 1989.
- [14] Carlos H. Crisosto. Stone fruit maturity indices: a descriptive review. *Postharvest News and Information*, 5:65N–68N, 1994.
- [15] B.I. Brown and R.B.H. Wills. Post-harvest changes in guava fruit of different maturity. *Scientia Horticulturae*, 19:237–243, 1983.
- [16] G.W. Chapman and R.J. Horvat. Changes in nonvolatile acids, sugars, pectin and sugar composition of pectin during peach (cv. monroe) maturation. *Journal of Agricultural Food Chemistry*, 38:383–387, 1990.
- [17] Stephen R. Harris. *Production is only half the battle: A training manual in fresh produce marketing for the Eastern Caribbean*. FAO, 1988.
- [18] A. Fekete, M. Nagy, and D. Kantor. Analysis of force-deformation relationship with fruits. In *2005 ASAE Annual International Meeting*. American Society of Agricultural Engineers (ASAE), 2005.

- [19] Christopher James Mils. Non-destructive testing of fruit firmness with real time constraints. Master's thesis, School of Computer Science and Software Engineering - Monash University, November 2005.
- [20] N. Laguado, E. Prez, C. Alvarado, and M. Marín. Características físico-químicas y fisiológicas de frutos de guayaba de los tipos criolla roja y san miguel procedentes de dos plantaciones comerciales. *Rev. Fac. Agron. (LUZ)*, 16:382–397, 1999.
- [21] Edmundo Mercado-Silva, Pedro Benito-Bautista, and María García-Velasco. Fruit development, harvest index and ripening changes of guavas produced in central Mexico. *Postharvest Biology and Technology*, 13:143–150, 1998.
- [22] Alfonso Parra and Jose Eugenio Hernandez. *Fisiología Postcosecha de Frutas y Hortalizas*. Universidad Nacional de Colombia, Santa Fe de Bogota, D.C., 1997.
- [23] A. Caizares, D. Laverde, and R. Puesme. Crecimiento y desarrollo del fruto de guayaba (*Psidium guajava* L.) en Santa Bárbara, Estado Monagas, Venezuela. *Revista UDO Agrícola*, 3(1):34–38, 2003.
- [24] Wikipedia. Refractometer — wikipedia, the free encyclopedia. Online resource: <http://en.wikipedia.org/w/index.php?title=Refractometer&oldid=152695805>, 2007. [Online; accessed 15-October-2007].
- [25] Luther R. Wilhelm, Dwayne A. Suter, and Gerald H. Brusewitz. *Food & Process Engineering Technology*, chapter 3. Texture of Food Materials, page 53. ASAE. ©American Society of Agricultural Engineers, 53-64. St. Joseph, Michigan, 2004.
- [26] G.S. Birth. *Quality Detection in Foods*, chapter How light interacts with foods, pages 6–11. ASAE. ©American Society of Agricultural Engineers, 53-64. St. Joseph, Michigan, 1976.
- [27] J.E. Lancaster, C.E. Lister, P.F. Reay, and C.M. Triggs. Influence of pigment composition on skin color in a wide range of fruits and vegetables. *J. Am. Soc. Hortic. Sci.*, 122:594–598, 1997.

- [28] Minolta. *Precise Color Communication*. Minolta Co., Ramsey, New Jersey, 1994.
- [29] Mauricio Reyes, David Rivas, Elena Montilla, and Efraín Solarte. Determinación del estado de maduración de tomates por métodos espectroscópicos. *Revista Colombiana de Física*, 38:241–244, 2006.
- [30] G.S. Birth, G.G. Dull, W.T. Renfro, and S.J. Kays. Nondestructive spectrophotometric determination of dry matter in onions. *J. Am. Soc. Hortic. Sci.*, 110:297–303, 1985.
- [31] D.C. Slaughter, D. Barrett, and M. Boersig. Nondestructive determination of soluble solids in tomatoes using near infrared spectroscopy. *Journal of Food Science*, 61:695, 1996.
- [32] W. R. Hruschka. *Near-Infrared Technology in the Agricultural and Food Industries*, chapter Data analysis: wavelength selection methods, pages 35–55. American Association of Cereal Chemists, St. Paul, MN, 1987.
- [33] J. A. Abbott. *Nondestructive Quality Evaluation of Horticultural Crops: Proceedings International Symposium on Nondestructive Quality Evaluation of Horticultural Crops, 24th International Horticulture Congress*, chapter Quality measurement by delayed light emission and fluorescence, pages 24–33. Saiwai Shobou Publishing Co., Tokyo, 1996.
- [34] P.M. Keagy, B. Parvin, and T.F. Schatzki. Machine recognition of navel orange worm damage in x-ray images of pistachio nuts. *Lebensm.-Wiss. Technol.*, 29:140–145, 1996.
- [35] B. Hills. *Magnetic resonance imaging in food science*. John Wiley & Sons Inc., New York, 1998.
- [36] Anette K. Thybo, Sune N. Jespersen, and Hans J. Stødkilde-Jørgensen Poul Erik Lærke. Nondestructive detection of internal bruise and spraing disease symptoms in potatoes using magnetic resonance imaging. *Magnetic Resonance Imaging*, 22:1311–1317, 2004.
- [37] R.W. Bajema, G.M Hyde, and A.L. Baritelle. Temperature and strain rate effects on the dynamic failure properties of potato tuber tissue. *Trans. Am. Soc. Agric. Eng.*, 41:733–740, 1998.

- [38] M.J. Delwiche, S. Tang, and J.J. Mehlschau. An impact force response fruit firmness sorter. *Trans. Am. Soc. Agric. Eng.*, 32:321–326, 1989.
- [39] M.J. Delwiche and Y. Sarig. A probe impact sensor for fruit firmness measurement. *Trans. Am. Soc. Agric. Eng.*, 34:187–192, 1991.
- [40] J. Sugiyama, K. Otobe, and Y. Kikuch. A novel firmness meter for fruits and vegetables. *Am. Soc. Agr. Eng.*, pages Paper 94–6030, 1994.
- [41] R. Lu and J.A. Abbott. Finite element modeling of transient responses of apples to impulse excitation. *Trans. Am. Soc. Agric. Eng.*, 40:1395–1406, 1997.
- [42] J.A. Abbott, D.R. Massie, B.L. Upchurch, and W.R. Hruschka. Non-destructive sonic firmness measurement of apples. *Trans. ASAE*, 38(5):1461–1466., 1995.
- [43] M.L. Stone, X. Zhang G.H. Brusewitz, and D.D. Chen. Watermelon maturity determination in the field with acoustic impedance techniques. *Am. Soc. Agric. Eng.*, pages Paper 94–024, 1994.
- [44] Jesús Brezmes, M. Luisa López-Fructuoso, Eduard Llobet, Xavier Vilanova, Inmaculada Recasens, Jorge Orts, Guillermo Saiz, and Xavier Correig. Evaluation of an electronic nose to assess fruit ripeness. *IEEE Sensors Journal*, 1:97–108, 2005.
- [45] Lessing Arturo Cárdenas, Rina Margarita Tirado, and Eduardo Gómez. *Visión por Computador*. Universidad Tecnológica de Bolívar, 2004. Monografía del Minor de Automatización Industrial.
- [46] J. Blasco, N. Aleixos, and E. Moltó. Computer vision detection of peel defects in citrus by means of a region oriented segmentation algorithm. *Journal of Food Engineering*, 81:535–543, 2007.
- [47] Corrado Di-Natale, Daniel Filippini, Giorgio Pennazza, Marco Santonico, Roberto Paolesse, Andrea Bellincontro, Fabio Mencarelli, Arnaldo DAmicoa, and Ingemar Lundström. Sorting of apricots with computer screen photoassisted spectral reflectance analysis and electronic nose. *Sensors and Actuators B*, 119:70–77, 2006.

- [48] Graphic Quality Consultancy. Introduction to colour spaces - cie lab and lch. Online resource:http://www.colourphil.co.uk/lab_lch_colour_space.html, 2007.
- [49] Joe Roberts. Noise reduction in digital (ccd and webcam) imaging. Online resource: <http://www.rocketroberts.com/astro/ccdnoise.htm>, 2003.
- [50] Mathworks. Matlab 7 r2006a, 2006. Natick, MA.
- [51] Linda G. Shapiro and George C. Stockman. *Computer Vision*. Prentice-Hall, New Jersey, 2001.
- [52] Greg Pass and Ramin Zabih. Histogram refinement for content-based image retrieval. *IEEE Workshop on Applications of Computer Vision*, pages 96–102, 1996.
- [53] D. Filippini, S. Svensson, and I. Lundström. Computer screen as a programmable light source for visible absorption characterization of (bio)chemical assays. *Chem. Commun.*, pages 240–241, 2003.
- [54] B P Singh, H K Singh, and K S Chauhan. Effect of post-harvest calcium treatments on the storage life of guava fruits. *Indian Journal of Agricultural Science*, 51(1):44–47, 1981.
- [55] A. Sharaf and S. S. El-Saadany. Biochemical studies on guava fruits during different maturity stages. *Annals of Agriculture Science*, 24(2):975–984, 1996.
- [56] Flavio Diniz Soares, Talita Pereira, Mrcia O. Maio-Marques, and Alciene R. Monteiro. Volatile and non-volatile chemical composition of the white guava fruit (*psidium guajava*) at different stages of maturity. *Food Chemistry*, 100:15–21, 2007.
- [57] A. P. Medlicott and M. J. Jeger. *Mangoes: a review*. Commonwealth Science Council, London, 1987.
- [58] H A Bashir, A Abu-Goukh, and A Abu-Bakr. Compositional changes during guava fruit ripening. *Food Chemistry*, 80:557–563, 2003.

- [59] S.N. Jha, Sangeeta Chopra, and A.R.P. Kingsly. Modeling of color values for nondestructive evaluation of maturity of mango. *Journal of Food Engineering*, 78:22–26, 2007.